# Fluorescence Analysis of Calmodulin Mutants Containing Tryptophan: Conformational Changes Induced by Calmodulin-Binding Peptides from Myosin Light Chain Kinase and Protein Kinase II†

Marie Chabbert,‡,§ Thomas J. Lukas,‖ D. Martin Watterson,‖ Paul H. Axelsen,‡ and Franklyn G. Prendergast*,‡

*Department of Biochemistry and Molecular Biology, Mayo Foundation, Rochester, Minnesota 55905, and Department of Pharmacology, Vanderbilt University, Nashville, Tennessee 37232*

*Received November 26, 1990; Revised Manuscript Received March 22, 1991*

ABSTRACT: Peptide-induced conformational changes in five isofunctional mutants of calmodulin (CaM), each bearing a single tryptophan residue either at the seventh position of each of the four calcium-binding loops (i.e., amino acids 26, 62, 99, and 135) or in the central helix (amino acid 81) were studied by using fluorescence spectroscopy. The peptides RS20F and RS20CK correspond to CaM-binding amino acid sequence segments of either nonmuscle myosin light chain kinase (nmMLCK) or calmodulin-dependent protein kinase II (CaMPK-II), respectively. Both steady-state and time-resolved fluorescence data were collected from the various peptide–CaM complexes. Steady-state fluorescence intensity measurements indicated that, in the presence of an excess of calcium, both peptides bind to the calmodulin mutants with a 1:1 stoichiometry. The tryptophans located in loops I and IV exhibited red-shifted emission maxima (356 nm), high quantum yields (0.3), and long average lifetimes (6 ns). They responded in a similar manner to peptide binding, by only slight changes in their fluorescence features. In contrast, the fluorescence intensity of the tryptophans in loops II and III decreased markedly, and their fluorescence spectrum was blue-shifted upon peptide binding. Analysis of the tryptophan fluorescence decay of the last mentioned calmodulins supports a model in which the equilibrium between two (Trp-99) or three (Trp-62) states of these tryptophan residues, each characterized by a different lifetime, was altered toward the blue-shifted short lifetime component upon peptide binding. Taken together, these data provide new evidence that both lobes of calmodulin are involved in peptide binding. Both peptides induced similar changes in the fluorescence properties of the tryptophan residues located in the calcium-binding loops, with the exception of calmodulin with Trp-135. For this last mentioned calmodulin, slight differences were observed. Tryptophan in the central helix responded differently to RS20F and RS20CK binding. RS20F binding induced a red-shift in the emission maximum of Trp-81 while RS20CK induced a blue-shift. The quenching rate of Trp-81 by iodide was slightly reduced upon RS20CK binding, while RS20F induced a 2-fold increase. These results provide evidence that the environment of Trp-81 is different in each case and are, therefore, consistent with the hypothesis that the central helix can play a differential role in the recognition of, or response to, CaM-binding structures.

Calmodulin (CaM)[1] is a ubiquitous protein involved in the regulation of a wide variety of calcium-dependent intracellular processes as varied as motivity, secretion, glycogen metabolism, synaptic transmission, transport of anions, and cyclic nucleotide metabolism [for reviews, see Rasmussen et al. (1984) and Manalan and Klee (1984)]. Upon calcium binding, calmodulin apparently undergoes conformational changes, which enable it to bind to and activate target enzymes such as calmodulin-stimulated phosphodiesterase, plasma membrane $Ca^{2+}$ pump, myosin light chain kinase, and calmodulin-dependent protein kinase II (Cox et al., 1984; Stoclet et al., 1987). The interaction of calmodulin with its target enzymes is very little known at the molecular level [for a review, see Blumenthal and Krebs (1988)]. It is thought that most calmodulin-dependent enzymes contain specific regions that recognize and bind to calmodulin with high affinity. Such putative calmodulin-binding sites have been found in, e.g., skeletal muscle myosin light chain kinase (Blumenthal et al., 1985), smooth muscle myosin light chain kinase (Lukas et al., 1986), calmodulin-dependent protein kinase II (Payne et al., 1988), nonerythroid $\alpha$-spectrin (Leto et al., 1989), or the $Ca^{2+}$ pump of human erythrocytes (James et al., 1988). Most of the peptides based on these sequences have the ability to form cationic amphiphilic helices. This structure seems to play a key role in calmodulin–target enzyme recognition (Cox et al., 1985; O'Neil et al., 1987). However, modifications in calmodulin, either by chemical reaction (Newton et al., 1984; Mann & Vanaman, 1988) or by site-directed mutagenesis (Putkey et al., 1986; Craig et al., 1987; Weber et al., 1989),

† Supported by NIH Grants GM34847 (to F.G.P.) and GM30861 (to D.M.W.).

* To whom correspondence should be addressed.

‡ Mayo Foundation.

§ Present address: CNRS UA 491, Faculté de Pharmacie, Université Louis Pasteur de Strasbourg, BP 24, F-67401 Illkirch Cedex, France.

‖ Vanderbilt University.

[1] Abbreviations: SYNCAM refers to an isofunctional mutant of calmodulin (CaM) whose sequence is a hybrid of the vertebrate and the plant calmodulins; T26W, T62W, S81W, F99W, and Q135W SYNCAMs refer to mutants of SYNCAM in which Thr-26, Thr-62, Ser-81, Phe-99, and Glu-135, respectively, were replaced by a tryptophan residue; the nucleotide and amino acid sequences reported in this paper can be obtained from the EMBL data bank under the accession number M11334; MLCK, myosin light chain kinase; smMLCK, smooth muscle MLCK; nmMLCK, nonmuscle MLCK; skMLCK, skeletal muscle MLCK; CaMPK-II, calmodulin-dependent protein kinase II; HEPES, *N*-(2-hydroxyethyl)piperazine-*N*′-2-ethanesulfonic acid; SDS, sodium dodecyl sulfate; EDTA, ethylenediaminetetraacetic acid.

0006-2960/91/0430-7615$02.50/0 

differentially affect the activation of various target enzymes. These observations suggest that calmodulin has more than one mode of binding to target enzymes.

Site-specific mutagenesis studies of both CaM and protein kinases (Weber et al., 1989; Shoemaker et al., 1990) demonstrate that there are differences as well as similarities in CaM interactions with myosin light chain kinase compared to those with calmodulin-dependent protein kinase II. For example, charge reversal mutations of CaM central helix residues affect smMLCK regulation but have little effect on CaMPK-II regulation. In contrast, similar mutations in a helix in the carboxy-terminal domain of CaM affect both enzymes (Weber et al., 1989). Chemical fragmentation, peptide analogue, and site-specific mutagenesis studies of nmMLCK and smMLCK have identified relatively short peptide segments (RS20 region) that are important for calmodulin binding and constitute the putative calmodulin-binding domain (Lukas et al., 1986; Shoemaker et al., 1990). Similar segments have also been identified in CaMPK-II (Payne et al., 1988). When the 20-residue long RS20 sequence of MLCK was replaced with the analogous sequence from CaMPK-II, the resulting enzyme was calmodulin dependent and acquired the calmodulin recognition properties of CaMPK-II (Shoemaker et al., 1990). On the basis of these considerations, the RS20 peptide analogue of the RS20 region of MLCK is a reasonable model to use for CaM binding to nmMLCK or smMLCK, and the corresponding sequence from CaMPK-II is a reasonable model for CaM/CaMPK-II recognition. The availability of peptide analogues of the CaM-binding sites of protein kinases provides a tractable experimental approach to study the molecular basis of CaM–target enzyme recognition.

We summarize here a study of the fluorescence properties of five isofunctional mutants of calmodulin, each of which contains a single tryptophan residue, in different structural domains, in the presence and absence of 20-residue calmodulin-binding peptides. The peptide sequences, based upon the amino acid sequence of nmMLCK (RS20F) or CaMPK-II (RS20CK), lack tryptophan or tyrosine residues and are, therefore, spectroscopically silent. Our purpose was to determine whether these peptides evoked similar or different effects on the host calmodulin molecule, to explain the differential responses of the two kinases to mutations in the central helix of calmodulin.

## Materials and Methods

*Chemicals.* All chemical were of reagent grade or better. High purity magnesium acetate and potassium chloride were purchased from Aldrich Chemical Co., HEPES and calcium chloride were from Serva. Acrylamide (Ultrapure grade) was from BMB. Ultrapure water (Sybron Instrument or Barnstead) was used throughout the experiments.

All experiments were performed in 50 mM HEPES, pH 7.5. The addition of other chemicals in the buffer will be specifically noted. The pH was adjusted to 7.50 ± 0.05, after correction for the temperature dependence of the p$K_a$ of the HEPES buffer. The temperature was controlled at 20 ± 1 °C.

*Calmodulin Mutants.* All calmodulins used in this study are derivatives of VU-1, or SYNCAM, calmodulin (Roberts et al., 1985; EMBL accession number M11334). F99W SYNCAM (previously named VU-9 calmodulin) was produced as described elsewhere (Kilhoffer et al., 1988) and can be found as an annotation to accession number M11334. The production of T26W, T62W, S81W, and Q135W SYNCAMs follows the general procedure described for several other calmodulin mutants (Craig et al., 1987; Roberts et al., 1987). They differ from SYNCAM by the replacement of a single residue, Thr-26, Thr-62, Ser-81, and Gln-135, respectively, by tryptophan. The nucleic acid sequences of the genes coding for these proteins was verified by automated DNA sequencing using techniques described previously (Zimmer et al., 1989). The DNA sequences of these mutants can also be found as an annotation to accession number M11334. As with F99W SYNCAM, these calmodulins were indistinguishable from VU-1 and vertebrate calmodulins in MLCK activator activity. Protein homogeneity was assessed by SDS–polyacrylamide gel electrophoresis and amino acid composition analysis. The calcium-saturated calmodulin mutants were stored at −80 °C, either lyophilized or in a buffer containing 50% glycerol. They were decalcified by using trichloroacetic acid precipitation (Haiech et al., 1981). The protein concentration was determined by UV spectrophotometry. The molar extinction coefficients at 280 nm were determined by taking the absorption spectrum of a given protein solution and measuring the protein concentration of the same sample by amino acid analysis.

*Peptide Preparation.* Peptides RS20F and RS20CK were assembled on a *p*-methylbenzhydrylamine resin (USB) in a Beckman synthesizer as described elsewhere (Lukas et al., 1986). They were purified by chromatography on carboxymethylcellulose (CM-52) in pH 5.5 ammonium acetate buffer, followed by reversed-phase HPLC (0.1% trifluoroacetic acid/acetonitrile) on a Waters μBondapak ODS column. After chromatography, peptide fractions were lyophilized and then redissolved in water. Peptide stock solutions in water were stored at −80 °C. Peptide concentrations were determined by amino acid analysis.

*Spectroscopic Methods.* UV absorption spectra were recorded on a Cary 219 spectrophotometer. Steady-state fluorescence measurements were performed with a MPF 66 spectrofluorimeter (Perkin-Elmer). The excitation wavelength was set at 295 nm to avoid contribution from Tyr-138. The quantum yields were determined relatively to that of tryptophan zwitterion at pH 7.0 (0.14). The protein concentration usually ranged between 2 and 20 μM.

Acrylamide quenching measurements were effected by adding aliquots of a concentrated stock solution of acrylamide to the protein solution in the presence or in the absence of peptides. The fluorescence intensity at 340 nm (emission slit of 5 nm) was measured at each acrylamide concentration. Fluorescence intensity values were corrected for the dilution and the screening effect due to the UV absorption of acrylamide at 295 nm and were then fitted according to the modified Stern–Volmer equation (Eftink & Ghiron, 1976):

$$I_0/I = (1 + K_{SV}[Q])e^{V[Q]} \quad (1)$$

in which $I_0$ and $I$ represent the 340-nm fluorescence intensity of the protein solution in the absence of acrylamide and at an acrylamide concentration [Q], respectively; $K_{SV}$ is the Stern–Volmer constant and $V$ is the static quenching constant. The fitting program was based on the Levenberg–Marquardt method (Bevington, 1986).

Iodide quenching measurements were performed at constant ionic strength by mixing various ratios of protein solutions containing either 150 mM KCl or 150 mM KI. The reciprocal of the fluorescence intensity, recorded at 350 nm, was linear and was fitted using a least-squares analysis procedure.

Fluorescence lifetime measurements were performed with the pulse fluorometry technique. Two similar systems, differing only in the origin of the laser excitation source (Coherent, Antares, or Spectra Physics Nd:YAG lasers) were used in this study. A complete description of the device has been

reported elsewhere (Hedstrom et al., 1988). Briefly, the mode-locked 1064-nm fundamental from the Nd:YAG laser was frequency doubled and used to synchronously pump a rhodamine 6G dye laser. The pulse repetition rate of the dye laser was controlled by a cavity dumper and set at 4 MHz. Output pulses, tuned at 295 nm, were up-converted with a frequency doubler employing an angle-tuned KDP crystal. Cavity-dumper output pulse widths (10-ps FWHM) were monitored continuously by using an autocorrelator. When necessary, incident laser intensities were attenuated by greater than an order of magnitude with neutral density filters. The UV pulses, initially horizontally polarized, were rotated to the magic angle before exciting the sample.

The emission was detected at right angle to the excitation beam with a Hamamatsu 1564U-03 microchannel plate. The emission wavelengths were selected with Schott interference filters with band-pass less than or equal to 10 nm or with a monochromator set at 5-nm band-pass (AmericanHolographic, Inc.). A Schott WG 320 filter was added in some measurements to eliminate most of the light scattering observable at wavelengths below 315 nm. The instrument response functions (Spectra Physics system, 90-ps FWHM; Coherent system, 50-ps FWHM) were obtained by collecting the scattered light at 295 nm from a nondairy creamer suspended in distilled water. The independence of the response function with emission wavelength was checked by measuring the lifetime of *p*-terphenyl in cyclohexane at various wavelengths.

Both for the sample decay and the response function, the counting was stopped when the peak channel reached 20000 counts. The calibration of the time-to-amplitude converter varied from 20 to 100 ps, depending upon the general features of the decay. The number of channels used in the fitting procedure varied from 512 to 992, depending on the calibration and the average lifetime of the decay, and was such that the number of counts in the last channel used for the fit was less than 2% of that of the peak channel.

The decay data were then analyzed as sums of exponentials:

$$I(t) = \sum_i \alpha_i e^{-t/\tau i} \qquad (2)$$

$$\text{with } \sum_i \alpha_i = 1$$

by an iterative reconvolution procedure based on the Marquardt algorithm. The number of exponentials was progressively increased until the fit did not improve. The adequacy of the fit was judged by the value of reduced $\chi^2$ and by visual inspection of weighted residuals and autocorrelation functions. In some cases, light scattering from the excitation pulse or Raman scattering of the solution added a very short component ($\tau < 40$ ps) to the fluorescence intensity decay. This additional component improved the $\chi^2$ dramatically but did not change the other components notably. In any event, its weight represented only a very few percent of the total fluorescence intensity. In these cases, we did not take this component into account and normalized the remaining preexponential factors to 1. For T62W SYNCAM, for which three discrete components were required to describe the decay throughout the spectrum (see below), the effects of light scattering were corrected for by the addition of a fourth component, whose lifetime was fixed at 10 ps. Most of the unconstrained fits with four components could not converge in an adequate number of iterations (99). Typical standard errors were calculated from two to five determinations.

Decay-associated spectra (DAS) were calculated from the steady-state fluorescence spectra and the multiexponential analysis of the decay data. The fluorescence associated to the component $i$ at the wavelength $\lambda$ was calculated from (Wahl & Auchet, 1972)

$$F_i(\lambda) = F(\lambda)\alpha_i(\lambda)\tau_i(\lambda)/\sum_j \alpha_j(\lambda)\tau_j(\lambda) \qquad (3)$$

*Computer-Generated Models.* Models of the five calmodulin mutants studied in this report were derived from the crystal structure for rat calmodulin provided by Babu et al. (1988) by using the molecular mechanics program CHARMM (Brooks et al., 1983; distributed by Polygen Corp., Waltham, MA). A total of 10 conservative mutations are required to change rat calmodulin into SYNCAM, plus one additional mutation for substituting Trp at five different sites. The procedure for generating mutant structure models was (1) copy atomic coordinates from the rat calmodulin structure into a new file for all atoms with identical IUPAC atom names in the desired mutant form; (2) build atom coordinates not provided in step 1 by using idealized internal geometry parameters; (3) subject the atoms generated in step 2 to 100 cycles of energy minimization (i.e., constrain all atomic coordinates copied from the original rat structure); (4) subject all atoms in each of the 11 mutated residues to an additional 100 cycles of energy minimization; and (5) subject the entire (unconstrained) structure to a final 100 cycles of energy minimization. The adapted basis Newton–Raphson energy minimization utility within CHARMM was used with an 8-Å nonbound cutoff and an explicit-hydrogen topology. This was applied to rationalize bond lengths, angles, and VDW overlaps. QUANTA (distributed by Polygen Corp., Waltham, MA) was used for graphical displays on an SGI 4D/120 GTX computer.

Three-dimensional electrostatic potential maps were generated with the "probe interaction" subroutine of QUANTA and a 1-Å probe with a charge of +1.0 atomic charge unit. The potential at each point of the maps corresponded to the electrostatic interaction between the probe and the atoms of the protein. The grid contours corresponding to −50 kcal/mol were generated. Intensity variations represented depth cueing. Atoms of the Trp side chains were removed prior to the calculations but then were restored for display purposes, along with the residues at positions cis-5, cis-9, trans-7, and trans-9 (see Discussion). Calcium-binding loops I–IV were graphically superimposed by least-squares minimization and photographed with the same view and perspective.

## Results

The sequences of peptides RS20F and RS20CK are given in Table I. The synthetic peptide RS20 is based on the amino acid sequence of the RS20 region of chicken fibroblast myosin light chain kinase (residues 1081–1100) (Shoemaker et al., 1990) or of chicken gizzard myosin light chain kinase (residues 494–513) (Lukas et al., 1986). It binds to calmodulin with very high affinity (Lukas et al., 1986). The synthetic peptide RS20F differs from RS20 in having a Phe residue substituted for Trp-4 in the naturally occurring target protein. This change in the sequence was necessary to eliminate the appearance of two Trp signals when peptide binding to the Trp-bearing calmodulins was studied. On the basis of the extensive mutagenesis studies of this region by Shoemaker et al. (1990), this change was not expected to result in a significant change in calmodulin regulation of MLCK. The synthetic peptide RS20CK is a 20-residue peptide that includes the proposed calmodulin-binding segment of the α-subunit of rat brain calmodulin-dependent protein kinase II. The minimal peptide based on the amino acid sequence of CaMPK-II to exhibit potent calmodulin-binding properties is 14 residues long and corresponds to the sequence of residues 296–309 of the

Table I: Sequences of Calmodulin-Binding Peptides Based on the Calmodulin-Binding Domains of Chicken Gizzard or Fibroblast Myosin Light Chain Kinase and of Calmodulin-Dependent Protein Kinase II

| peptide code | sequence |
|---|---|
| RS20 | R-R-K-W-Q-K-T-G-H-A-V-R-A-I-G-R-L-S-S-S[a] |
| RS20F | R-R-K-F-Q-K-T-G-H-A-V-R-A-I-G-R-L-S-S-S[b] |
| RA14CK | R-R-K-L-K-G-A-I-L-T-T-M-L-A[c] |
| RS20CK | R-R-K-L-K-G-A-I-L-T-T-M-L-A-T-R-N-F-S-S[d] |

[a] Calmodulin-binding peptide based on the amino acid sequence of residues 494–513 of chicken gizzard myosin light chain kinase (Lukas et al., 1986) or that of residues 1081–1100 of chicken fibroblast myosin light chain kinase (Shoemaker et al., 1990). [b] Synthetic peptide studied in this report and based on the sequence of RS20, with the substitution of Trp-4 by Phe. [c] Calmodulin-binding peptide based on the amino acid sequence of residues 296–309 of the α-subunit of calmodulin-dependent protein kinase II (Payne et al., 1988; Hanley et al., 1988). This peptide is the smallest peptide based on the sequence of this enzyme to exhibit potent calmodulin-binding properties. [d] Synthetic peptide studied in this report, based on the sequence of residues 296–315 of the α-subunit of calmodulin-dependent protein kinase II.

α-subunit (Payne et al., 1988; Hanley et al., 1988). Although these peptides share limited sequence identities, both are potent inhibitors of the calmodulin activation of MLCK and calmodulin activable phosphodiesterase (data not shown). On the basis of these considerations, the two peptide analogues were selected as spectroscopically silent models of the calmodulin–kinase interactions.

*Design Consideration.* The mutated CaMs studied in this report were engineered to have fluorescent probes positioned in each calcium-binding loop (seventh position) and in the central helix (position 81). All of the Trp residues had the potential of reporting different features of the protein–peptide interaction across the entire calmodulin molecule. Three-dimensional structures of the single Trp-containing mutants of calmodulin were built based on the X-ray crystallographic structure of calmodulin (Babu et al., 1988; data set 3CLN of the Brookhaven Protein Data Base), as described under Materials and Methods. The modeling analyses indicated that model structures for the five calmodulin mutants retain all secondary structure elements reported for rat calmodulin by Babu et al. (1988). The molecular graphics depictions indicated that, as Tyr-99 in rat calmodulin, the tryptophans positioned in the calcium-binding loops could be exposed to the solvent and were located on the opposite side of the hydrophobic clefts in calmodulin (not shown). Trp-81 could potentially report interactions of peptides with the central helix of calmodulin.

Inspection of the energy-minimized models revealed that substitution of Trp for the seventh residue in each EF-hand loop does not distort the calcium binding site geometry and does not interfere with coordination of the main chain C=O of this residue to calcium ions as found in the crystal structure (Babu et al., 1988). In the crystal structure of rat calmodulin, the N–H groups of Thr-26 and Gln-135 appear to associate with the single coordinated carboxylate groups of Asp-24 and Asp-133, respectively, pointing most directly at the oxygen that coordinates to the calcium in each case. In contrast, the N–H groups of Thr-62 and Tyr-99 hydrogen-bond to the side-chain carbonyl groups of Asn-60 and Asn-97, respectively. The N–H groups of the Trp substituted to these residues could be stabilized similarly. Trp side chains in each loop appear able to contact the main-chain carbonyl oxygens of Gly residues in position 6 and the hydrogen-bonding atoms of Ile and Val residues at position 8. They are adjacent to the water molecule coordinated to the calcium ion. In addition, they are each situated at the amino end of an α-helix. Helix dipole effects, if any, would likely be greatest for Trp-62 at the end of the long central helix.

Table II: Spectroscopic Features of the Trp-Containing SYNCAMs, in the Absence or in the Presence of Peptides RS20F or RS20CK[a]

| SYNCAM | conditions | $\lambda_{max}$ (nm) | $A/A_0$ | $\Phi$ |
|---|---|---|---|---|
| T26W | 1 mM $Ca^{2+}$ | 356 | 1 | 0.32 |
| | +RS20F | 356 | 0.86 | |
| | +RS20CK | 356 | 0.87 | |
| T62W | 1 mM $Ca^{2+}$ | 349 | 1 | 0.12 |
| | +RS20F | 341 | 0.50 | |
| | +RS20CK | 341 | 0.53 | |
| S81W | 1 mM $Ca^{2+}$ | 344 | 1 | 0.19 |
| | +RS20F | 346 | 1.43 | |
| | +RS20CK | 337 | 1.70 | |
| F99W | 1 mM $Ca^{2+}$ | 350 | 1 | 0.14 |
| | +RS20F | 347 | 0.69 | |
| | +RS20CK | 346 | 0.65 | |
| Q135W | 1 mM $Ca^{2+}$ | 356 | 1 | 0.31 |
| | +RS20F | 356 | 0.93 | |
| | +RS20CK | 354 | 0.85 | |

[a] The experiments were performed in 50 mM HEPES, pH 7.5, and 1 mM $Ca^{2+}$, at 20 °C. The excitation wavelength was set at 295 nm. $\lambda_{max}$ represents the wavelength of the fluorescence emission maximum; $A$ is the total fluorescence intensity of the protein, based on the integration of the spectrum from 300 to 500 nm; $A_0$ is the total fluorescence intensity of the same protein in the absence of added peptides; $\Phi$ is the quantum yield of the protein, measured by comparison to that of tryptophan zwitterion at pH 7.0. The concentration of the calmodulin mutants and of the added peptides were the same as in Figure 1, except for the measurements of the quantum yields, which were carried out with protein concentrations around 15 μM.

The residues in positions 7 and 9 of each calcium-binding loop are involved in short twisted β-sheet structures, although only the residues in position 8 actually form hydrogen bonds (Babu et al., 1988). The sheet forms the base of a shallow rift between the two loops. Trp-26 and Trp-62 situate in the rift between loops I and II; Trp-99 and Trp-135 situate between loops III and IV. The interdomain rift is shallow and sufficiently wide to permit considerable though not complete rotational freedom for the Trp side chains. Because of this rotational freedom, it is not possible to predict specific interactions between the tryptophans positioned in the loops and other residues.

Electrostatic potential maps, generated as described under Materials and Methods, are shown in Figure 1. The grid contours corresponding to −50 kcal/mol are displayed. They indicate that the area within them has a negative electrostatic potential and illustrate the pattern of negatively charged groups in the vicinity of each tryptophan residue. The similarity of the distributions of electrostatic charges in the vicinity of Trp-26 and Trp-135 correlate with their spectroscopic similarity (see below). Trp-62 and Trp-99 each display unique spectral behavior and likewise appear to have unique electrostatic environment (see below).

Finally, the Trp-81 side chain, situated in the middle of the central helix, is rotationally unhindered and should be easily accessible to solvent. This residue is in a region of high negative electrostatic potential (Weber et al., 1989). Its environment is dominated by the negatively charged side chains of Asp-78, Asp-80, Glu-82, and Glu-84 (not shown).

*Steady-State Fluorescence Properties of the Trp-Containing SYNCAMs and SYNCAM–Peptide Complexes.* The goal of this study was to characterize the interactions of the calcium–calmodulin complex with the two model peptides. Therefore, initial steady-state analysis of the mutant calmodulins was done in the presence of calcium and in the presence or absence of each peptide. Table II summarizes the key spectral features of the mutated calmodulins, in the presence of 1 mM calcium. The excitation wavelength was 295 nm,

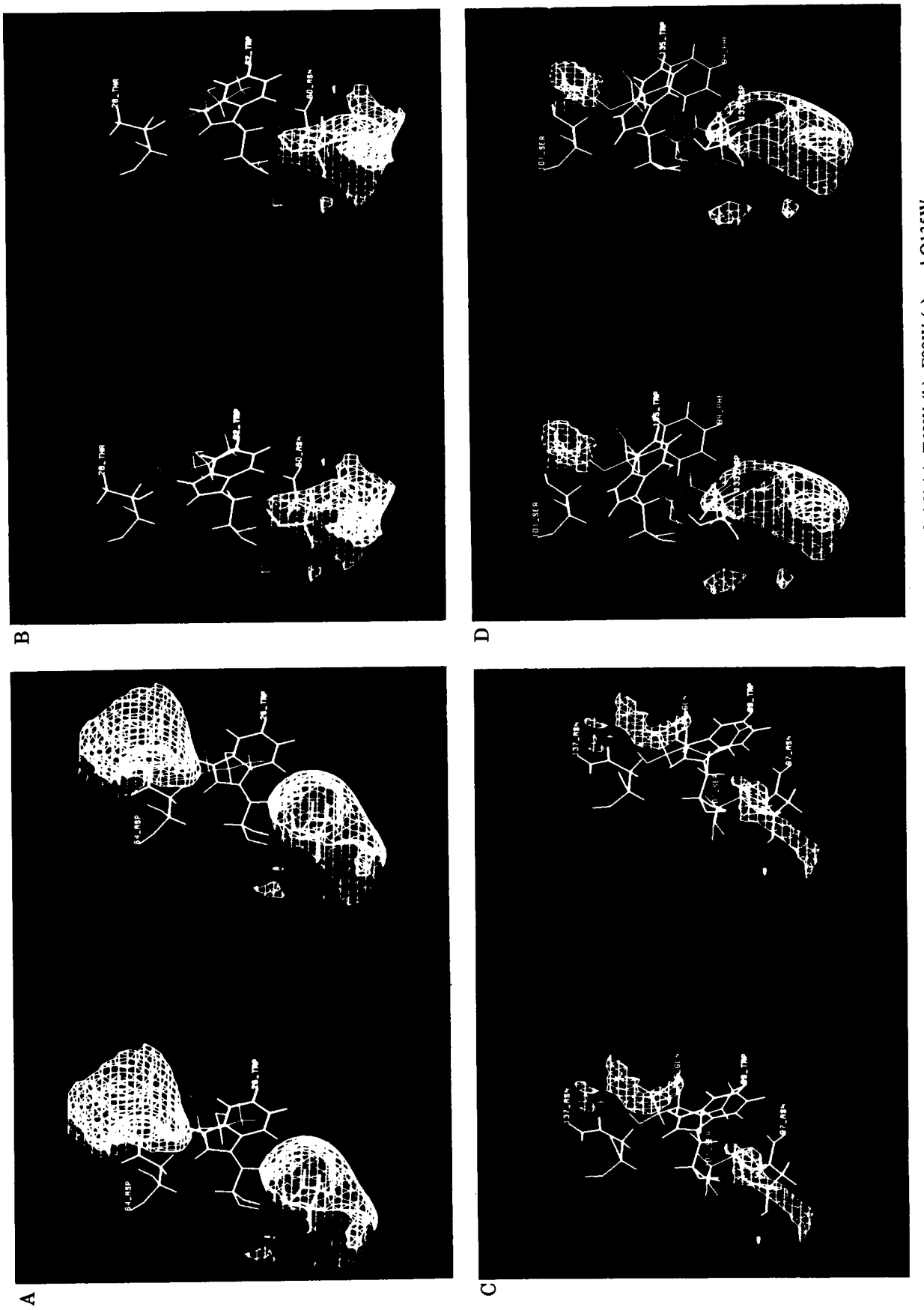


FIGURE 1: Stereoviews of the electrostatic potential maps of the tryptophan environment in T26W (a), T62W (b), F99W (c), and Q135W (d) SYNCAMs. The maps were generated as described under Materials and Methods. The grid contours correspond to an electrostatic potential of −50 kcal/mol.

to selectively excite the tryptophan residue and avoid fluorescence from Tyr-138.

The emission maximum of T26W and Q135W SYNCAMs was 356 nm, similar to that of Trp zwitterion in water, as determined experimentally with our device. Their quantum yields were about 0.3, which is much higher than Trp in water. The emission maximum of T62W SYNCAM (349 nm) and that of F99W SYNCAM (350 nm) were similar, with quantum yields (0.12 and 0.14) comparable to that of Trp in water. The emission maximum of S81W SYNCAM was blue-shifted compared to Trp in water (344 nm) and its quantum yield was higher (0.19). These spectral features of the Trp-containing SYNCAMs are in good agreement with those determined elsewhere (Kilhoffer et al., 1989; Kilhoffer, personal communication).

The fluorescence of each Trp-containing calmodulin was significantly affected by both peptides (Figure 2 and Table II). The stoichiometry of each complex was determined by monitoring the total fluorescence intensity of the protein as a function of the peptide/protein ratio. Figure 3 shows an example of these results for S81W and F99W SYNCAMs. In all cases, the fluorescence intensity changes were proportional to the molar ratio of peptide to protein until this ratio was equal to 1.0 ± 0.1. Further addition of peptide did not change the fluorescence intensity. The titration curve was independent of protein concentration over a 10-fold concentration range (from 2 to 20 $\mu$M). These data suggest strongly that RS20F and RS20CK bind to calmodulin with a 1:1 stoichiometry, although we cannot exclude spectroscopically silent interactions. Moreover, the stoichiometric binding of either peptide to the Trp-containing SYNCAMs that is observed under our experimental conditions, demonstrates that the association constant is greater than $10^6$ M and that differential responses to peptide binding cannot be related to differences in binding affinity.

To examine the role of calcium in this binding, we repeated some of these fluorescence measurements with RS20F in the absence of calcium. In this case, the apparent stoichiometry of the binding depended on the mutated calmodulin investigated. For example, the fluorescence intensity of calcium-free F99W SYNCAM in the presence of RS20F plotted versus the peptide/protein ratio is sigmoidal (Figure 4) and strongly suggests the formation of a 2:1 complex, as observed in the case of, e.g., melittin in the absence of calcium (Maulet & Cox, 1983). On the other hand, the spectral changes of S81W SYNCAM suggest a 1:1 complex between RS20F and S81W SYNCAM in the absence of calcium (not shown). Importantly, in the presence of calcium, we did not observe 2:1 complexes between RS20F or RS20CK and any of the five mutated calmodulins investigated, which supports the inference of a 1:1 stoichiometry in these conditions.

The spectral characteristics of the single Trp-containing calmodulins in the complexes with peptides RS20F and RS20CK are summarized in Table II and demonstrate the different features of the complexes. The fluorescence intensity of the tryptophans located in any of the four calcium-binding loops (positions 26, 62, 99, and 135) decreased upon peptide binding. The effect of the peptides on the fluorescence intensity was relatively small for T26W and Q135W SYNCAMs and much larger for T62W and F99W SYNCAMs. The binding of either peptide induced a similar decrease in the fluorescence intensity of T26W SYNCAM and did not change its emission maximum. The two peptides had slightly different effects on the spectral features of Q135W SYNCAM. RS20F binding did not change the emission maximum but slightly decreased the fluorescence intensity. In contrast, RS20CK induced a small but reproducible 2-nm blue-shift in the emission maximum and a larger decrease in the fluorescence intensity. The binding of either peptide induced a 8-nm blue-shift in the emission maximum of T62W SYNCAM and a 3–4-nm blue-shift in that of F99W SYNCAM. It is noteworthy that, whenever a shift in the fluorescence spectrum was observed, this shift was to the shorter wavelengths.

The spectral features of S81W SYNCAM were differentially changed by the two peptides. The binding of RS20F induced a slight but reproducible red-shift of the emission maximum and that of RS20CK a marked blue-shift. The fluorescence intensity increased by 43% in the presence of RS20F and by 70% in the presence of RS20CK. Both peptides narrowed the fluorescence emission spectral width of S81W SYNCAM. Its spectral width at half-maximum was 63 nm in the absence of peptide, compared to 61 nm for tryptophan zwitterion at pH 7.0. Upon peptide binding, it decreased to 59 (RS20CK) or 61 nm (RS20F).

*Time-Resolved Fluorescence of the Tryptophans in T26W and Q135W SYNCAMs and SYNCAM–Peptide Complexes.* Fluorescence decays were analyzed as sums of exponentials as described under Materials and Methods. Table III reports the analysis of the decay of T26W and Q135W SYNCAMs in the presence and absence of peptides at three wavelengths. Whatever the emission wavelength, the decay of T26W SYNCAM was dominated by a long component whose weight represented at least 85% of the total fluorescence intensity. This dominant component had a 6.8-ns lifetime at 350 nm and seemed only marginally dependent on the emission wavelength. The lifetime of the shorter component increased from 1.4–1.5 ns on the blue edge of the spectrum to 3–4 ns on the red edge, while its preexponential factor decreased from 0.45 at 315 nm to 0.20 at 410 nm. The addition of peptides RS20F or RS20CK did not change these general features significantly (Table III).

The reduced contribution of the short-lived component and, on the red edge of the spectrum, a ratio of the long decay time to the short one of around 2, made the resolution of the shorter decay difficult. Because of the marked increase in $\tau_1$ throughout the spectrum, we suspect that additional decay times cannot be resolved. The decrease in reduced $\chi^2$ from the blue edge to the red edge of the spectrum is consistent with this assumption. These decay times could result from ground-state heterogeneities or excited-state processes. An alternative explanation could be that the species related to the short component undergoes a dipolar relaxation phenomenon during the excited-state lifetime (Lackowicz & Cherek, 1980). In either case, the short lifetime observed would correspond to a combination of other decay rates. Because of their reduced weight, these components marginally affect the overall decay of Trp-26, and, thus, we did not attempt to better characterize them.

The fluorescence intensity decay of Q135W SYNCAM was very similar to that of T26W SYNCAM (Table III) and echoes the similarity of their steady-state spectral features. The addition of peptide RS20F did not significantly change the decay, and only a slight decrease in the average lifetime was observed. RS20CK binding induced a small but reproducible decrease in the preexponential factor of the longer component, e.g., from 0.79 to 0.70 at 350 nm. In every case, the preexponential factor of the shorter component decreased from the blue edge to the red edge of the spectrum. The spectrum associated with the short component was blue-shifted, as compared to that of the long component. The increase in

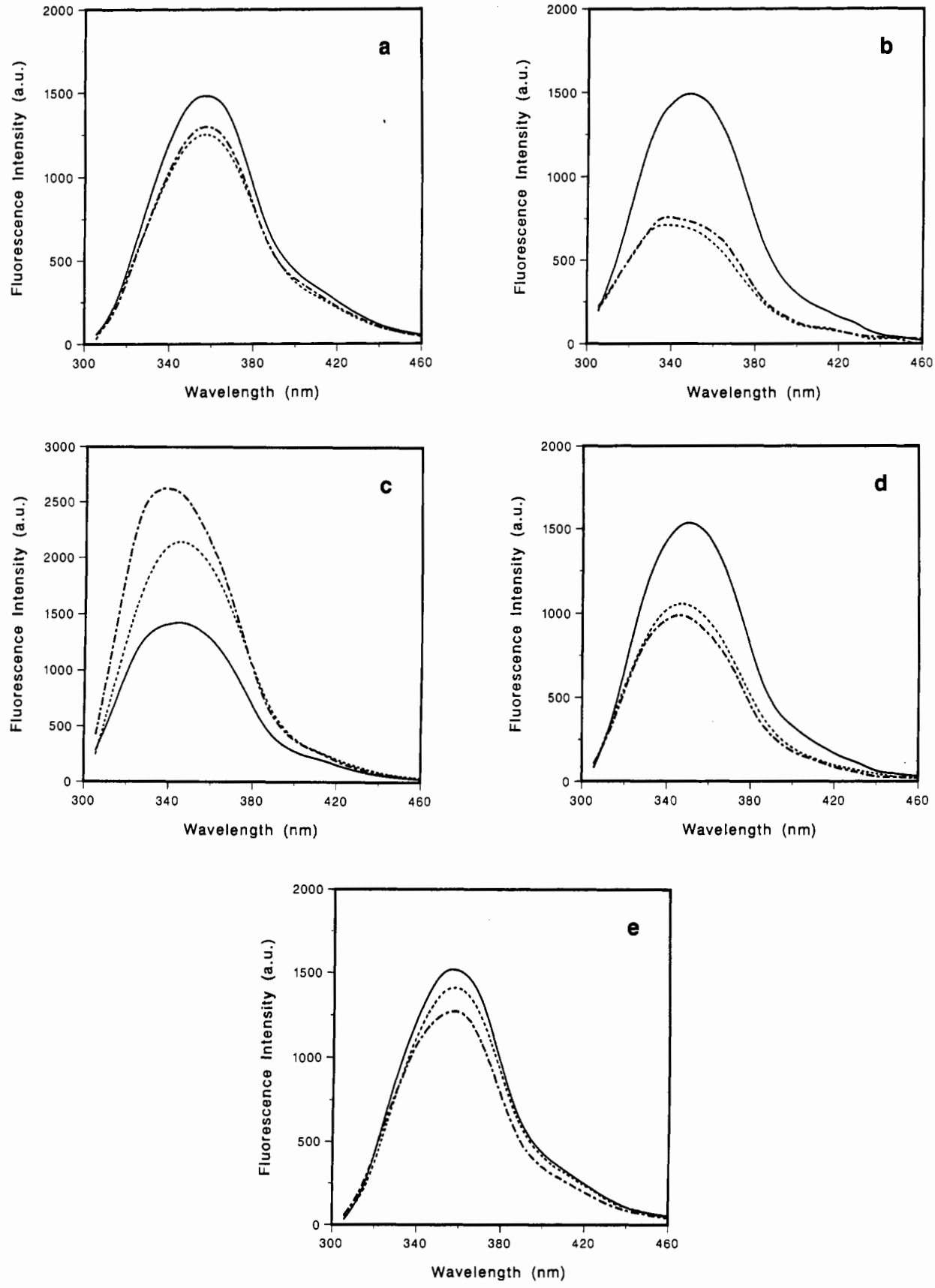


FIGURE 2: Effect of RS20F and RS20CK binding on the steady-state fluorescence spectra of the Trp-containing mutants of calmodulin, in the presence of calcium. The proteins were either free (—) or complexed to RS20F (- - -) or to RS20CK (- - -). (a) T26W SYNCAM; when present, the molar ratio of peptide to protein was 1.9 (RS20CK) or 2.1 (RS20F); (b) T62W SYNCAM, molar ratio 1.7 (RS20CK) or 2.7 (RS20F); (c) S81W SYNCAM, molar ratio 1.8 (RS20CK) or 2.1 (RS20F); (d) F99W SYNCAM, molar ratio 2.6 (RS20CK) or 1.9 (RS20F); (e) Q135W SYNCAM, molar ratio 2.3 (RS20CK) or 2.1 (RS20F). The calmodulin concentration ranged from 1.7 to 3.3 $\mu$M in the different experiments. The fluorescence intensity was normalized to have the same area for the spectrum of every protein in the absence of added peptide. The spectra were corrected for the contribution of the buffer. The experiments were performed in 50 mM HEPES, pH 7.5, and 1 mM $Ca^{2+}$. The excitation wavelength was 295 nm.

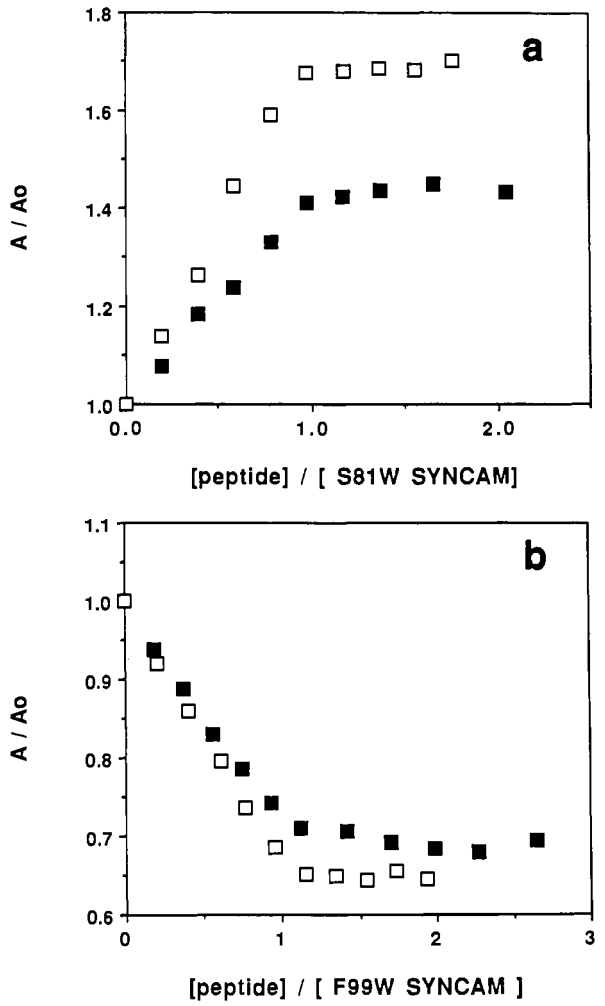


FIGURE 3: Determination of the stoichiometry of peptides RS20F or RS20CK binding to mutated calmodulins, in the presence of calcium. The relative fluorescence intensity of a solution of S81W SYNCAM (a) or F99W SYNCAM (b) is plotted as a function of the molar ratio of added peptide RS20F (closed square) or RS20CK (open square) to calmodulin. The relative fluorescence intensities are based upon integration of emission spectra from 300 to 500 nm. The concentration of S81W SYNCAM was 3.2 $\mu$M in the presence of RS20F or 2.6 $\mu$M in the presence of RS20CK. That of F99W SYNCAM was 3.3 $\mu$M in the presence of RS20F or 2.6 $\mu$M in the presence of RS20CK. The experiments were performed in 50 mM HEPES, pH 7.5, and 1 mM $Ca^{2+}$.

the amplitude of this short component upon peptide RS20CK binding might explain the blue-shift observed and would be consistent with the hypothesis that the two components correspond to different species of the tryptophan residue.

From the quantum yields (Table II) and the decay parameters of Trp-26 and Trp-135 at the emission maximum (Table III), we could estimate the radiative decay rates, $k_r$, of these tryptophans with (Werner & Forster, 1979)

$$\Phi = k_r(\sum_i \alpha_i \tau_i) \qquad (4)$$

This led to an estimate of $k_r$ of $0.055 \times 10^9$ $s^{-1}$ for Trp-26 and $0.052 \times 10^9$ $s^{-1}$ for Trp-135. These values are in good agreement with that of $0.050 \times 10^9$ $s^{-1}$ calculated for the radiative decay rate of *N*-acetyl-L-tryptophanamide in water (Werner & Forster, 1979), indicating that the very high quantum yields observed for these residues are related to reduced nonradiative decay rates and not to a drastic alteration of the electronic structure of their singlet state.

*Time-Resolved Fluorescence of the Tryptophans in T62W and F99W SYNCAMs and SYNCAM–Peptide Complexes.*

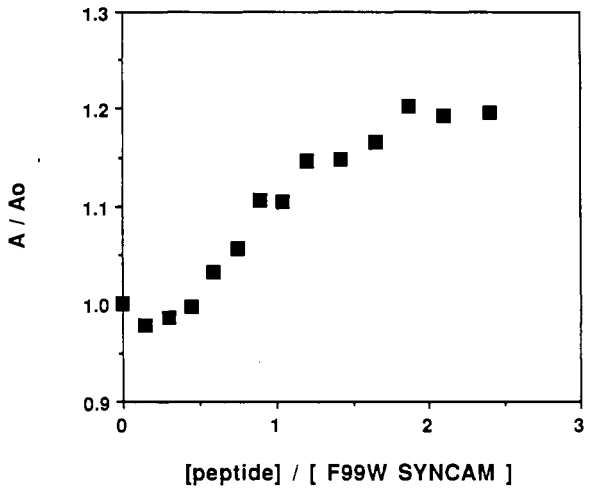


FIGURE 4: Relative fluorescence intensity of F99W SYNCAM as a function of added peptide RS20F, in the absence of calcium. The relative fluorescence intensity is based upon integration of emission spectrum. The concentration of F99W SYNCAM was 10 $\mu$M. EDTA was added to the sample to a final concentration of 0.2 mM. The experiments were performed in 50 mM HEPES, pH 7.5.

Whatever the emission wavelength at which the decay was measured, at least three components were required to give an acceptable fit of the fluorescence decay of the tryptophan residue in calcium-saturated T62W SYNCAM, either in the absence or in the presence of the peptides (Table IV). Attempts to fit the 350-nm decay of T62W SYNCAM with a biexponential law led to a reduced $\chi^2$ of around 4. A $\chi^2$ of 1.3 was obtained when a third component was added in the reconvolution procedure. The decay times that described the fluorescence decay of T62W SYNCAM in the absence of peptide were independent of the emission wavelength and averaged at 5.2 ± 0.1, 1.7 ± 0.2, and 0.58 ± 0.08 ns, over 10 wavelengths spanning the spectrum. The preexponential factor of the 1.7-ns component was independent of the emission wavelength, while that of the 5.2-ns component increased from the blue edge to the red edge of the spectrum and that of 0.6-ns component decreased. When 1:1 complexes were formed with RS20F or RS20CK, the lifetimes of the three components that described the decay were similar to those observed in the absence of peptide. The mean of the subnanosecond component lifetime over 10 different wavelengths spanning the spectrum was 0.55 ± 0.04 ns in the presence of RS20F and 0.49 ± 0.04 ns in the presence of RS20CK. The lifetime $\tau_2$ averaged at 1.6 ± 0.2 ns in the presence of RS20F and 1.5 ± 0.1 ns in the presence of RS20CK. Upon binding of either peptide, the longer lifetime increased slightly with the emission wavelength to plateau at 5.2 ± 0.2 ns at wavelengths ≥370 nm. Despite the similarities of the lifetimes, major changes were observed in the preexponential factors of the longest and shortest components. At 350 nm, the preexponential factor of the 5-ns component decreased by 70% from 0.30 to 0.09 upon peptide binding, whereas that of the subnanosecond component increased from 0.46 to more than 0.60. The preexponential factor for the second component did not change significantly (from 0.25 to 0.28).

Table V summarizes an analysis of the decay of F99W SYNCAM at three different emission wavelengths. Either in the absence or in the presence of peptides RS20F and RS20CK, two components described the fluorescence intensity decay at $\lambda \geq 340$ nm. At 310 nm, the addition of a third component, in the subnanosecond range, improved the fit. We cannot exclude that some light-scattering contamination may be concealed in this short component. However, the actual

Table III: Analysis of a Typical Fluorescence Decay of T26W and Q135W SYNCAMs, at Various Wavelengths, in the Absence or in the Presence of Added Peptides RS20F or RS20CK[a]

| SYNCAM | conditions | λ (nm) | $\tau_1$ (ns) | $\alpha_1$ | $\tau_2$ (ns) | $\alpha_2$ | $\bar{\tau}$ (ns) | $\chi^2$ |
|---|---|---|---|---|---|---|---|---|
| T26W | 1 mM $Ca^{2+}$ | 315 | 6.2 | 0.57 | 1.4 | 0.43 | 4.1 | 2.2 |
| | | 350 | 6.8 | 0.78 | 2.1 | 0.22 | 5.8 | 1.8 |
| | | 410 | 7.2 | 0.80 | 3.4 | 0.20 | 6.4 | 1.3 |
| | +RS20F | 315 | 6.1 | 0.57 | 1.4 | 0.43 | 4.1 | 2.1 |
| | | 350 | 6.6 | 0.81 | 2.2 | 0.19 | 5.8 | 1.8 |
| | | 410 | 7.0 | 0.77 | 4.0 | 0.23 | 6.3 | 1.2 |
| | +RS20CK | 315 | 6.1 | 0.56 | 1.4 | 0.44 | 4.0 | 2.1 |
| | | 350 | 6.6 | 0.81 | 2.2 | 0.19 | 5.8 | 1.7 |
| | | 410 | 7.1 | 0.76 | 4.0 | 0.24 | 6.3 | 1.2 |
| Q135W | 1 mM $Ca^{2+}$ | 315 | 6.6 | 0.42 | 1.7 | 0.58 | 3.8 | 1.6 |
| | | 350 | 6.9 | 0.79 | 2.1 | 0.21 | 5.9 | 1.3 |
| | | 410 | 6.9 | 0.89 | 2.7 | 0.11 | 6.4 | 1.2 |
| | +RS20F | 315 | 6.0 | 0.42 | 1.5 | 0.58 | 3.4 | 1.9 |
| | | 350 | 6.5 | 0.78 | 2.1 | 0.22 | 5.5 | 1.2 |
| | | 410 | 6.8 | 0.83 | 3.2 | 0.17 | 6.2 | 1.2 |
| | +RS20CK | 315 | 6.4 | 0.35 | 2.0 | 0.65 | 3.5 | 2.1 |
| | | 350 | 6.7 | 0.69 | 2.1 | 0.31 | 5.3 | 1.3 |
| | | 410 | 7.1 | 0.79 | 3.2 | 0.21 | 6.3 | 1.2 |

[a] The fluorescence decays of T26W and Q135W SYNCAMs were analyzed as sums of exponentials. Below 340 nm, the $\chi^2$ value was considerably reduced by the addition of a third component in the fitting procedure (from more than 4 to about 2). The third component was very short ($\tau$ <40 ps) and was attributed to Rayleigh and Raman scattering. For these wavelengths, we took into account only the two main components obtained with a triexponential analysis. Their preexponential terms were normalized to have a sum equal to 1. The concentration of T26W SYNCAM was 9 μM and that of Q135W SYNCAM was 16 μM. The molar ratio of peptide to calmodulin was 1.4. The measurements were performed in 50 mM HEPES, pH 7.5, in the presence of 1 mM $Ca^{2+}$. The average of the lifetimes is defined by $\bar{\tau} = \sum_i \alpha_i \tau_i$. Typical standard errors were ±0.1 for $\tau_1$ throughout the spectrum. They increased from the blue edge to the red edge of the spectrum for $\tau_2$, from ±0.2 to ±0.5, and for $\alpha_1$ and $\alpha_2$, from ±0.02 to ±0.05.

Table IV: Multiexponential Analysis of a Typical Fluorescence Decay of T62W SYNCAM at Various Wavelengths, in the Absence or in the Presence of Added Peptides[a]

| conditions | λ (nm) | $\tau_1$ (ns) | $\alpha_1$ | $\tau_2$ (ns) | $\alpha_2$ | $\tau_3$ (ns) | $\alpha_3$ | $\bar{\tau}$ (ns) | $\chi^2$ |
|---|---|---|---|---|---|---|---|---|---|
| 1 mM $Ca^{2+}$ | 310 | 5.1 | 0.14 | 2.0 | 0.25 | 0.67 | 0.61 | 1.6 | 1.2 |
| | 350 | 5.2 | 0.30 | 1.6 | 0.24 | 0.51 | 0.46 | 2.2 | 1.3 |
| | 390 | 5.3 | 0.37 | 1.8 | 0.23 | 0.59 | 0.40 | 2.6 | 1.2 |
| +RS20F | 310 | 4.2 | 0.06 | 1.8 | 0.28 | 0.59 | 0.66 | 1.1 | 1.2 |
| | 350 | 4.6 | 0.09 | 1.4 | 0.28 | 0.52 | 0.64 | 1.1 | 1.2 |
| | 390 | 5.4 | 0.11 | 1.7 | 0.26 | 0.55 | 0.63 | 1.4 | 1.3 |
| +RS20CK | 310 | 4.0 | 0.07 | 1.6 | 0.29 | 0.54 | 0.64 | 1.1 | 1.2 |
| | 350 | 4.9 | 0.09 | 1.4 | 0.29 | 0.46 | 0.61 | 1.1 | 1.6 |
| | 390 | 5.3 | 0.12 | 1.6 | 0.29 | 0.49 | 0.59 | 1.4 | 1.3 |

[a] The contamination of the fluorescence decay by Raman or Rayleigh scattering below 340 nm could be corrected by the addition of a fourth component in the fitting procedure, whose lifetime was constrained to 10 ps. At these wavelengths, we took into account the results obtained for the three main components of the decay, using the four exponential analysis of the data. The measurements were performed in 50 mM HEPES, pH 7.5, in the presence of 1 mM $Ca^{2+}$. The concentration of T62W CaM was 17 μM and the molar ratio of peptide to calmodulin 1.5. The average of the lifetimes is defined by $\bar{\tau} = \sum_i \alpha_i \tau_i$. Typical standard errors were for $\tau_1$, ± 0.1, for $\tau_2$, ±0.2, for $\tau_3$, ±0.1 in the absence of peptide or ±0.05 in the presence of peptide, and for $\alpha_1$, $\alpha_2$, and $\alpha_3$, ±0.01.

Table V: Multiexponential Analysis of a Typical Fluorescence Decay of F99W SYNCAM in the Absence and in the Presence of Added Peptides[a]

| conditions | λ (nm) | $\tau_1$ (ns) | $\alpha_1$ | $\tau_2$ (ns) | $\alpha_2$ | $\tau_3$ (ns) | $\alpha_3$ | $\bar{\tau}$ (ns) | $\chi^2$ |
|---|---|---|---|---|---|---|---|---|---|
| 1 mM $Ca^{2+}$ | 310 | 6.6 | 0.10 | 1.5 | 0.90 | | | 2.0 | 4.2 |
| | | 7.3 | 0.07 | 1.7 | 0.66 | 0.29 | 0.27 | 1.7 | 1.5 |
| | 350 | 7.4 | 0.22 | 1.7 | 0.78 | | | 3.0 | 1.6 |
| | 390 | 7.5 | 0.26 | 1.7 | 0.74 | | | 3.2 | 1.5 |
| RS20F | 310 | 5.6 | 0.05 | 1.4 | 0.95 | | | 1.6 | 4.3 |
| | | 6.4 | 0.03 | 1.6 | 0.70 | 0.17 | 0.28 | 1.4 | 1.9 |
| | 350 | 7.2 | 0.09 | 1.6 | 0.91 | | | 2.1 | 1.4 |
| | 390 | 7.1 | 0.13 | 1.6 | 0.87 | | | 2.3 | 1.8 |
| RS20CK | 310 | 4.7 | 0.06 | 1.5 | 0.94 | | | 1.7 | 4.5 |
| | | 5.7 | 0.02 | 1.7 | 0.71 | 0.20 | 0.26 | 1.3 | 1.5 |
| | 350 | 6.0 | 0.07 | 1.7 | 0.93 | | | 2.0 | 1.6 |
| | 390 | 6.0 | 0.14 | 1.7 | 0.86 | | | 2.3 | 1.4 |

[a] The decay was analyzed as sums of exponentials. In all the cases, the concentration of F99W CaM was 11 μM. When peptide RS20F or RS20CK was present, its molar ratio to calmodulin was 1.3. The measurements were performed in 50 mM HEPES, pH 7.5, and 1 mM $Ca^{2+}$, with an excitation wavelength set at 295 nm. The average of the lifetimes is defined by $\bar{\tau} = \sum_i \alpha_i \tau_i$. Typical standard errors were for $\tau_1$, ±0.2, for $\tau_2$, ±0.1, for $\tau_3$, ±0.1, and for $\alpha_i$, ±0.01.

value found for this short lived species, 0.2 ± 0.1 ns, strongly suggests a physical origin in the protein for this component. This component represented only about 5% of the total fluorescence intensity at 310 nm, which did not allow us to characterize it more precisely. Most of the fluorescence decay could be described by two components. In the absence of peptide, the lifetimes of these components were 7.4 ± 0.1 and 1.7 ± 0.1 ns. These results are similar to those reported

Table VI: Effect of the Addition of 5 mM Magnesium Acetate and 100 mM Potassium Chloride on the 340-nm Fluorescence Decay of F99W SYNCAM[a]

| conditions | | $\tau_1$ (ns) | $\alpha_1$ | $\tau_2$ (ns) | $\alpha_2$ | $\chi^2$ |
|---|---|---|---|---|---|---|
| 1 mM $Ca^{2+}$ | | 7.6 | 0.19 | 1.7 | 0.81 | 1.4 |
| | +5 mM $Mg^{2+}$ | 7.5 | 0.20 | 1.6 | 0.80 | 1.6 |
| | +100 mM KCl | 7.5 | 0.19 | 1.7 | 0.81 | 1.6 |
| | +5 mM $Mg^{2+}$ + 100 mM KCl | 7.4 | 0.21 | 1.7 | 0.79 | 1.5 |
| +RS20F | | 7.4 | 0.07 | 1.5 | 0.93 | 1.4 |
| | +5 mM $Mg^{2+}$ | 7.5 | 0.07 | 1.5 | 0.93 | 1.5 |
| | +100 mM KCl | 7.6 | 0.07 | 1.5 | 0.93 | 1.7 |

[a] The measurements were performed in 50 mM HEPES, pH 7.5, and 1 mM $Ca^{2+}$. The concentration of F99W CaM was 12.5 $\mu$M. When peptide RS20F was present, its molar ratio to calmodulin was 1.5. The ionic concentration of the buffer was changed by adding an aliquot of a stock solution of magnesium acetate or potassium chloride. The excitation wavelength was 295 nm, and the emission wavelength was 340 nm.

Table VII: Multiexponential Analysis of a Typical Fluorescence Decay of S81W SYNCAM at 350 nm, in the Absence or in the Presence of Added Peptides RS20F or RS20CK[a]

| conditions | $\tau_1$ (ns) | $\alpha_1$ | $\tau_2$ (ns) | $\alpha_2$ | $\bar{\tau}$ (ns) | $\chi^2$ |
|---|---|---|---|---|---|---|
| 1 mM $Ca^{2+}$ | 5.7 | 0.52 | 1.8 | 0.48 | 3.8 | 1.8 |
| +RS20F | 6.3 | 0.69 | 2.4 | 0.31 | 5.1 | 1.4 |
| +RS20CK | 6.4 | 0.69 | 2.8 | 0.31 | 5.3 | 1.4 |

[a] The concentration of S81W CaM was 20 $\mu$M. When the peptides were present, their molar ratio to calmodulin was 1.5. The experiments were performed in 50 mM HEPES, pH 7.5, and 1 mM $Ca^{2+}$. The average lifetime is defined by $\bar{\tau} = \sum_i \alpha_i \tau_i$. Typical standard errors were for $\tau_1$, ±0.2, for $\tau_2$, ±0.2, and for $\alpha_i$, ±0.02.

Table VIII: Quenching of the Fluorescence of S81W CaM by Acrylamide and Iodide, in the Presence and Absence of Peptides RS20F or RS20CK[a]

| quencher | conditions | $K_{SV}$ ($M^{-1}$) | $k_q$ ($M^{-1}s^{-1}$) | $V$ ($M^{-1}$) |
|---|---|---|---|---|
| acrylamide | | 5.9 | $1.2 \times 10^9$ | 1.2 |
| | +RS20F | 5.9 | $1.0 \times 10^9$ | 0.9 |
| | +RS20CK | 4.7 | $0.8 \times 10^9$ | 0.1 |
| iodide | | 1.8 | $0.37 \times 10^9$ | |
| | +RS20F | 3.9 | $0.68 \times 10^9$ | |
| | +RS20CK | 1.8 | $0.31 \times 10^9$ | |

[a] Quenching measurements were performed in 50 mM HEPES, pH 7.5, and 1 mM $Ca^{2+}$, by measuring the fluorescence intensity of S81W CaM, in the absence or in the presence of added peptides, as a function of the concentration of quencher. The concentration of S81W CaM was between 2 and 3 $\mu$M and, when the peptides were present, their molar ratio to calmodulin was 1.3. The acrylamide concentration was increased by adding aliquots of a 3.75 M stock solution. The iodide quenching experiments were carried out at constant ionic strength by mixing various ratios of protein solutions containing either 150 mM KCl or 150 mM KI. The data are the average of at least two experiments. Data analysis was performed as described under Materials and Methods.

previously (Chabbert et al., 1989). The shorter lifetime was not altered significantly upon peptide binding. At 350 nm, the longer lifetime did not change markedly when peptide RS20F was added to F99W SYNCAM, while the binding of peptide RS20CK induced a decrease to 6.0 ns (Table V). A slight dependence of $\tau_1$ upon the emission wavelength was observed on the blue edge of the spectrum in the presence of RS20F. As for T32W SYNCAM, despite the similarities in the lifetimes, major changes occurred in the preexponential factors of the two components upon peptide binding. At 350 nm, the preexponential factor of the long component decreased from 0.22 to about 0.08 when either peptide bound to F99W SYNCAM. This corresponds to a decrease in the fluorescence intensity weight of this component from about 50 to about 20%.

The effect of ion concentration and of the presence of magnesium ions was also determined. An analysis of the fluorescence decay of F99W SYNCAM at 340 nm, when 5 mM $Mg^{2+}$ or 150 mM KCl was added to the reaction mixture, in the presence or in the absence of peptide RS20F, is summarized in Table VI. No changes were observed. Similar results were obtained for various wavelengths, spanning the spectrum from 305 to 410 nm (not shown).

Continuous lifetime distributions have been proposed as an alternative model to describe fluorescence decay of tryptophan in proteins (Alcala et al., 1987a,b). With phase fluorimetry, attempts to analyze Trp-99 decay with continuous lifetime distributions led to narrow distributions centered on the lifetimes actually found by using discrete components (not shown). This corroborates the assumption of a physical meaning for these decay components (see below).

*Fluorescence Properties of S81W SYNCAM and SYNCAM-Peptide Complexes.* The fluorescence decay of S81W SYNCAM fluorescence at 350 nm could be described as the sum of two exponentials (Table VII). The decay was dominated by a long component that represented about 80% of the fluorescence intensity. Using eq 4, we could estimate a radiative decay rate of $0.05 \times 10^9$ $s^{-1}$, similar to that of *N*-acetyl-L-tryptophanamide in water, from the average of the lifetimes at 350 nm ($\sum_i \alpha_i \tau_i = 3.8$ ns) and the quantum yield (0.19, cf. Table II). Peptide binding induced an increase in the two lifetimes and in the preexponential factor of the long component, leading to an increase in the average of the lifetimes. The higher increases in the fluorescence intensities (Table II) could be related to a red-shift in the absorption spectrum, which induces a significant increase in the optical density at 295 nm (the excitation wavelength). Analysis of the fluorescence decay at different wavelengths gave results similar to those reported at 350 nm (not shown). In contrast to T62W and F99W SYNCAMs (see Discussion), the fluorescence decay of S81W SYNCAM could not give direct key to understand the changes in the fluorescence properties of S81W SYNCAM upon peptide binding.

Fluorescence-quenching experiments were employed in an attempt to better characterize the environment of this residue, both in the absence and in the presence of peptides. Acrylamide and iodide quenching measurements were carried out as described under Materials and Methods. In the absence of peptide as well as in the presence of RS20F, the Stern–Volmer plot of the quenching of S81W SYNCAM fluorescence by acrylamide showed a marked upward curvature, indicating a static quenching component (Figure 5a). This effect was much smaller in the presence of RS20CK. The data were fit according to eq 1, and the best fits are reported in Table VIII. The dynamic quenching rate $k_q$ was defined by $k_q = K_{SV}/\langle\tau\rangle$ where $\langle\tau\rangle$ represents the average lifetime defined as $\langle\tau\rangle = (\sum_i \alpha_i \tau_i^2)/(\sum_i \alpha_i \tau_i)$ and $K_{SV}$ is the Stern–Volmer constant. The quenching rate of S81W SYNCAM by acrylamide in the absence of peptide, $1.2 \times 10^9$ $M^{-1}$ $s^{-1}$, was characteristic of a tryptophan residue partially buried (Eftink & Ghiron, 1976). Typically, the rate constant for acrylamide quenching of tryptophan in protein ranges from $4 \times 10^9$ $M^{-1}$ $s^{-1}$ for a fully exposed tryptophan to less than $0.5 \times 10^9$ $M^{-1}$ $s^{-1}$ for a fully buried residue (Eftink & Ghiron, 1976). Under

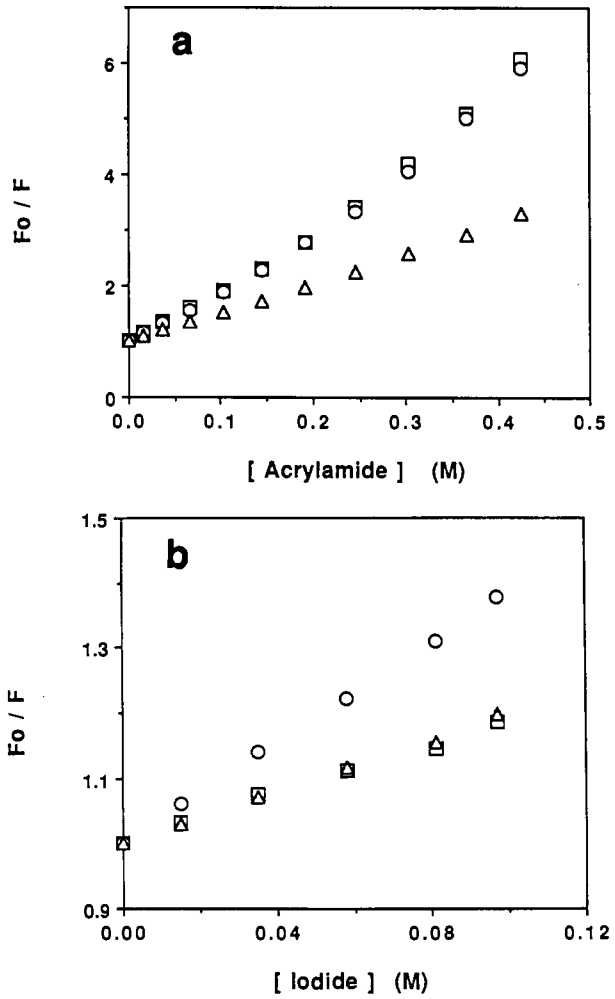


FIGURE 5: Stern–Volmer plot of the quenching of S81W SYNCAM by acrylamide (a) and iodide (b), in the absence of peptide (square) and in the presence of RS20F (circle) or of RS20CK (diamond). The experiments were performed as described under Materials and Methods. $I_0$ represents the fluorescence intensity in the absence of quencher and $I$ in its presence. The emission wavelength was 340 (acrylamide) or 350 nm (iodide) (emission slit, 5 nm). The fluorescence intensities were corrected for the buffer contribution, and, in the case of acrylamide, for dilution and the screening effect due to the optical density of acrylamide at the excitation wavelength. The acrylamide quenching experiments were carried in 50 mM HEPES, pH 7.5, and 1 mM $Ca^{2+}$, by adding aliquots of acrylamide. The concentration of S81W SYNCAM was 2.3 $\mu$M. The iodide quenching experiments were carried out with [S81W CaM] = 2.8 $\mu$M, at constant ionic strength, by mixing various ratios of protein solutions containing either 150 mM KCl or 150 mM KI, in 50 mM HEPES, pH 7.5. When the peptides were present, their molar ratio to calmodulin was 1.3.

similar conditions (50 mM HEPES, pH 7.5, 1 mM $Ca^{2+}$), the quenching rate of F99W SYNCAM by acrylamide was 2.2 $\times$ $10^9$ $M^{-1}$ $s^{-1}$ (Kilhoffer et al., 1989). In contrast, the static quenching constant, 1.2 $M^{-1}$, is high for a Trp side chain partially buried and suggests that acrylamide molecules may be trapped in the environment of Trp-81. The dynamic quenching rate of Trp-81 by acrylamide was not significantly altered by RS20F. It was slightly reduced to 0.8 $\times$ $10^9$ $M^{-1}$ $s^{-1}$ by RS20CK. The static quenching component was markedly reduced by RS20CK binding, suggesting that steric factors decrease markedly the probability that an acrylamide molecule is, at the time of excitation, sufficiently close to the indole side chain to make the probability of quenching 1.0 (Lackowicz, 1983a).

The Stern–Volmer plots of S81W SYNCAM quenching by iodide were linear (Figure 5b). The quenching rate by iodide was strongly reduced as compared to that by acrylamide (0.37 $\times$ $10^9$ $M^{-1}$ $s^{-1}$), probably reflecting electrostatic repulsions by negative charges (mainly Asp-78 and Glu-84) close to Trp-81. It decreased slightly upon RS20CK binding. In contrast, RS20F induced a marked 2-fold increase in this quenching rate. This strongly suggests the existence of electrostatic interactions in the complex calmodulin–RS20F yielding a neutralization in part of the negative charges surrounding residue 81. These data imply that the structures of the SYNCAM–RS20F and SYNCAM–RS20CK complexes are different in the environment of residue 81.

## Discussion

Whenever one studies mutated proteins, especially with spectroscopic techniques, the question of their structural identity to the wild-type protein inevitably, but justifiably, arises. Without either crystallographic or high-resolution NMR data for each mutant, we cannot verify structural identity, and spectroscopic data must be interpreted with some caution. In our study of the five Trp-containing SYNCAMs described above, there are some mitigating circumstances. First and foremost, the mutated forms of calmodulin are isofunctional with wild-type calmodulin across a broad spectrum of target enzymes. Secondly, the inferences drawn from the molecular graphics depictions are reassuring. Our computer models were generated by using the X-ray determined crystal structure of rat calmodulin (Babu et al., 1985, 1988) and molecular mechanics based minimization. The overall structure of the calmodulin mutants so generated coveraged excellently (and not surprisingly) with that of the wild-type protein. Given these considerations, the rest of our discussion focuses on what the fluorescence data allow us to infer regarding the structural basis for peptide binding and the effects of peptide binding on the conformation of calmodulin. In addition, the physical basis for the fluorescence properties themselves must be considered.

*Fluorescence Properties of T26W and Q135W SYNCAMs.* The fluorescence data appear to distinguish T26W and Q135W SYNCAMs apart from T62W and F99W SYNCAMs in four ways: (1) the quantum yields are about twice as large, (2) their average lifetimes are longer, (3) the maximum emission wavelengths are longer, and (4) the effects of peptides on the fluorescence intensity are relatively small. The quantum yield and the average lifetime of these tryptophans are strikingly large compared to those usually observed for a tryptophan residue in a protein [for a review, see Beechem and Brand (1985)]. As previously observed, the high quantum yields correlate well with the lifetimes, suggesting that a quenching mechanism of the tryptophan fluorescence which usually occurs in proteins cannot occur in the case of T26W and Q135W SYNCAMs.

Symmetry features of the four calcium-binding loops suggest that we describe the side-chain environment in terms of loop position (1–12) and whether a residue is in the same loop as the substituted Trp ("cis") or in the adjacent loop ("trans"). Molecular graphics reveal several differences between the environments of Trp-26 and Trp-135, such as different residues in cis-9 (Thr-28 vs Asn-137), trans-7 (Thr-62 vs Phe-99), and trans-9 (Asp-64 vs Ser-101) positions (Figure 1). However, in view of their similar photophysical behavior, we note that the electrostatic potential maps show similarities in the distribution of charges in their environment (Figure 1). Moreover, Trp-26 and Trp-135 have two structural features in common that are not found in the other mutants: (1) the main-chain N–H group is apparently stabilized by the coordinated carboxylate oxygen at the cis-5 position of the calcium

binding loop; and (2) the indole moiety may collide with the uncoordinated carboxylate oxygen of the same residue.

For tryptophan and peptides with a N-terminal tryptophanyl residue, a deprotonated amino group gives rise to red-shifted emission spectra, higher quantum yield, and longer fluorescence decay compared with the protonated form (Chang et al., 1983; Petrich et al., 1983). The effect of pH on the quantum yield of Trp fluorescence can be mimicked by complex formation between the amino group and 18-crown-6 (Shizuka et al., 1988), but in this case no emission shift was observed. The nonradiative processes proposed to explain the quenching by the ammonium group involve either a charge transfer from the indole ring to the adjacent carbonyl or $COO^-$ groups (Chang et al., 1983) or the proton transfer from protonated amino group to the indole ring (Shizuka et al., 1988).

A peptide bond at the amino end of tryptophan also induces an efficient quenching of tryptophan fluorescence (Werner & Forster, 1979; Chang et al., 1983). Following Ricci and Nesta (1976), these authors propose that this quenching results from the formation of an excited-state charge transfer complex between indole and the amide carbonyl group. The N–H groups of residues 26 and 135 are involved in H-bonds with carboxylate groups of Asp-24 and Asp-133. The presence of negative charges in the environment of the N–H group might reduce the efficiency of the carbonyl group to quench Trp fluorescence. Alternatively, the N–H of the indole moiety might form H-bonds with the uncoordinated carboxylate oxygen of these Asp residues. Further studies are required before a definite conclusion can be reached.

*Effect of Peptide Binding on the Fluorescence of T62W and F99W SYNCAMs.* Multiexponential decay of a tryptophan residue in a protein might be due to dipolar relaxation of the protein matrix around the tryptophan residue, ground-state heterogeneities, or excited-state reactions. The time-resolved fluorescence spectra of F99W SYNCAM in the presence of calcium (Chabbert et al., 1989) clearly exhibited an isosbestic point, which ruled out a continuous dipolar relaxation mechanism (Bakhshiev et al., 1965). The spectrum of F99W SYNCAM extrapolated at time $t = 0$ from the decay data ($\lambda_{max}$ = 340 nm) was markedly shifted as compared to a Trp residue in a proteic apolar environment, e.g., azurin (Finazzi-Agro et al., 1970). This indicates that the emission observed stems from excited states that are largely dipolarly relaxed. Dipolar relaxation is, thus, too fast to be observed with our device, which is consistent with the solvent exposure of this residue. The subnanosecond component observed on the blue edge of the spectrum and/or the slight increase in the longer lifetime with the emission wavelength in some conditions might be related to dipolar relaxation (Lackowicz & Cherek, 1980). These phenomena, however, only marginally affect the overall fluorescence decay observed.

The analysis of the fluorescence decay of F99W SYNCAM during calcium titration (Chabbert et al., 1989) showed that this decay was consistent with a two-state model in which the interconversion rates between the two excited states decreased upon calcium binding. The existence of an equilibrium between two "species" of Trp-99 is also suggested by $^1H$ NMR spectroscopy (M. Chabbert, B. D. Ray, M. D. Kemple, D. M. Watterson, and F. G. Prendergast, to be published elsewhere).

When the excited states do not interconvert, the system is equivalent to independent components: the decay times observed correspond to the intrinsic lifetimes of each state, and the preexponential factors are proportional to the ground-state fraction of each species (Lackowicz, 1983b; Alcala et al., 1987a). Major changes were observed in the preexponential factors of F99W SYNCAM fluorescence decay upon RS20F binding, whereas the decay times were not markedly altered (Table V). This result corresponds thus to that expected for a noninterconverting 2-state model, when the equilibrium constant between the two ground-state species is altered.

The changes in the ratio of the two components upon RS20CK binding are very similar to those observed for RS20F and suggest a similar shift of the equilibrium between the two conformations. The additional decrease in the long lifetime of F99W SYNCAM upon RS20CK binding could be related to a specific effect of this peptide. It is noteworthy that the ionic strength of the solution (at least up to 100 mM KCl) or the presence of 5 mM magnesium does not change the equilibrium.

We calculated the decay-associated spectra (DAS) for F99W SYNCAM in the absence and in the presence of peptides, as described under Materials and Methods. As the intensity weight of the subnanosecond component was in any case less than 5% of the total fluorescence intensity, we did not take it into account to calculate the decay-associated spectra. The spectra associated to the two main components are shown in Figure 6. At the spectral resolution of our measurements, their emission maxima are independent of the presence of the peptide, which corroborates the assumption that the changes observed in the fluorescence decay are related to a shift in the equilibrium between two states. That of the long lifetime component is red-shifted ($\lambda_{max}$ = 350 nm) as compared to that of the short lifetime component ($\lambda_{max}$ = 340 nm). The blue-shift in the steady-state spectrum upon peptide binding (Table II) may be related to the decrease in the weight of the long component. The decrease in the quantum yield (Table II) adequately matches the decrease in the average of the lifetimes around the emission maximum (e.g., 350 nm, cf. Table V) and is consistent with the model proposed.

The same approach was applied to T62W CaM. The wavelength independence of the three decay times that describe its fluorescence decay suggests that it may be possible to ascribe a physical meaning to the mathematically resolved individual decay components and that the same number of states, defined by a different lifetime, may exist. The spectra associated to each of the three components of the decay were calculated (not shown). The longest lifetime component had the most red-shifted spectrum ($\lambda_{max}$ = 350 nm), while the shortest lifetime component had the most blue-shifted spectrum ($\lambda_{max}$ = 330–340 nm). As for F99W SYNCAM, peptide binding induced a shift from the longest to the shortest lifetime states, which induced a blue-shift in the steady-state fluorescence spectrum and a decrease in the quantum yields (Table II).

The previous study of F99W SYNCAM (Chabbert et al., 1989) has shown qualitatively that the equilibrium between the two states of Trp-99 was shifted to the blue-shifted short lifetime component upon calcium binding. The binding of peptide RS20F or RS20CK induced a further shift of this equilibrium to this component. It is noteworthy that peptide binding to T62W SYNCAM induced also a shift to the blue-shifted short lifetime state of Trp-62, suggesting that the same situation might apply. The parallel effects of peptide and calcium binding on the equilibrium of the two lifetime defined states of Trp-99 correlate with the observation that different peptides induce an increase in the affinity of calmodulin for calcium (Olwin & Storm, 1985; Yazawa et al., 1987). Seeholzer and Wand (1989) have shown by $^1H$ NMR that the binding of a calmodulin-binding peptide from skMLCK to calmodulin stabilizes the structure of the globular

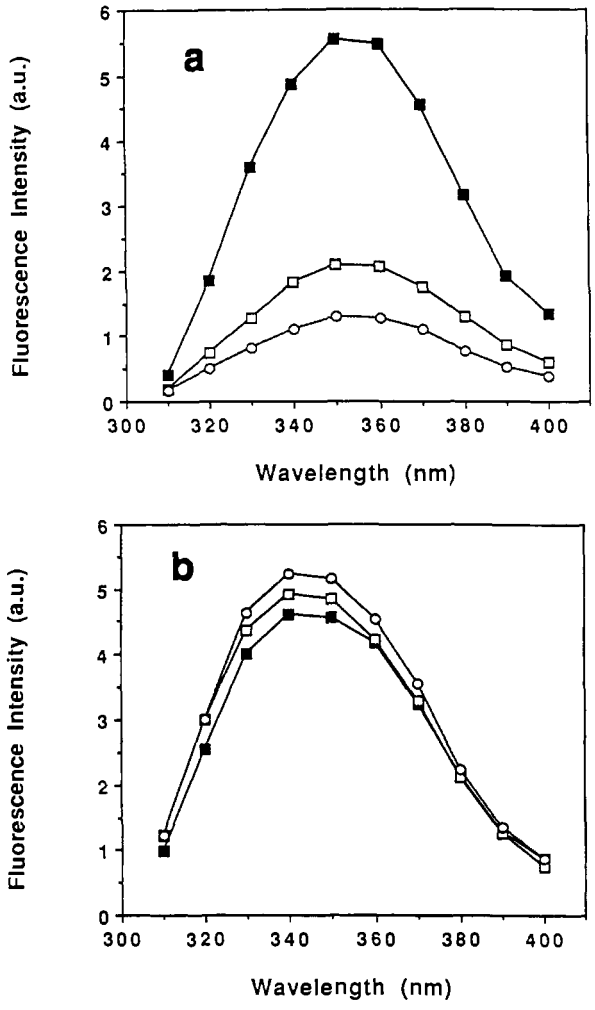


FIGURE 6: Decay-associated spectra of F99W SYNCAM. The spectra associated to the long component are reported in panel a, while those associated to the short one are reported in panel b. F99W SYNCAM was either free in solution (closed square) or complexed with RS20F (open square) or RS20CK (open circle). The concentration of F99W SYNCAM was 15 $\mu$M and the molar ratio of peptide to protein was 1.5. The relative fluorescence intensity of each component was calculated from the results of the biexponential analysis of F99W SYNCAM decay, as described under Materials and Methods.

domains in $Ca^{2+}$-bound calmodulin. The exchange rates of the amide NH located in the antiparallel sheet structures between the calcium-binding loops were significantly slower in the presence of peptide than in its absence. This increase in stability has been related to the decrease in free energy associated with complex formation. In particular, peptide binding induced a decrease in the exchange rates of the amide hydrogens of Thr-62 and Tyr-99 (Seeholzer & Wand, 1989). It would be tempting to speculate that the lifetime-defined conformations are related to the existence of a specific H-bond in the environment of the Trp residue and that the shift to the short-lifetime species is related to a stronger H-bond. However, we cannot make this conclusion in the absence of further information. Because of the rotational freedom for Trp side chains, the computer-generated models yielded little insight into the nature of these states. Their physical significance is presently under investigation.

*Peptide-Binding Mechanism.* Early reports have suggested that the exposure of hydrophobic regions upon calcium binding is key for calmodulin binding to target enzymes (LaPorte et al., 1980; Tanaka & Hidaka, 1980). The resolution of the three-dimensional structure of crystallized calmodulin (Babu et al., 1985, 1988; Kretzinger et al., 1988) indicates that a large hydrophobic cleft exists in each lobe of the molecule. The possibility of complex formation between calmodulin-binding peptides such as mastoparans and the C-terminal proteolytic fragment of calmodulin (Malencik & Anderson, 1984; Sanyal et al., 1988) has initially supported a mechanism in which the C-terminal moiety of calmodulin is involved in peptide binding. The flexible structure of the central helix has been evidenced by X-ray scattering (Heidorn & Trewhella, 1988) or site-directed mutagenesis (Persechini et al., 1988) experiments. This led Persechini and Kretzinger (1988) to propose a calmodulin-binding mechanism, based on molecular graphics, in which, due to the flexibility of the central helix, the two domains can be significantly closer than in the crystal structure and the hydrophobic clefts of both lobes can be involved simultaneously in the binding of $\alpha$-helical amphiphilic peptides. The compactness of calmodulin–peptide complex upon binding of calmodulin-binding peptides that are predicted to form basic amphiphilic helices, as MLCK-I based on skeletal muscle MLCK calmodulin-binding domain (Heidorn et al., 1989) or PhK5 from the catalytic subunit of skeletal muscle phosphorylase kinase (Trewhella et al., 1990), has been evidenced by X-ray and neutron-scattering experiments. Moreover, using photoreactive model peptides, O'Neil and DeGrado (1990) have provided experimental evidence that a peptide bearing two photolabels (positions 3 and 13) can interact simultaneously with the two hydrophobic clefts.

NMR studies have shown that amino acids in both halves of calmodulin are altered by peptide binding (Klevit et al., 1985; Linse et al., 1986; Yazawa et al., 1987; Seeholzer & Wand, 1989). In particular, Seeholzer and Wand (1989) have shown changes in the chemical shifts of any of the amino acids located at the seventh position of each calcium-binding loop upon peptide binding. Changes in the fluorescence behavior of the Trp residues in each of the four $Ca^{2+}$-binding loops upon peptide binding is not by itself surprising. However, the similarities in the fluorescence changes between Trp-26 (loop I) and Trp-135 (loop IV) and between Trp-62 (loop II) and Trp-99 (loop III) were not expected. The disposition of each hydrophobic cleft with respect to the central helix is different (Babu et al., 1988). Our results strongly support the inference that the two lobes exert a concerned effect and are involved directly in peptide binding.

These tryptophans are located in the opposite side of the hydrophobic clefts in calmodulin. Therefore, if these hydrophobic clefts are involved in peptide–calmodulin complex formation as strongly suggested by recent data (O'Neil et al., 1989; O'Neil & DeGrado, 1990), the tryptophan residues are not expected to be in close proximity to the peptide. In addition, the similarities in the effects observed between the N- and C-terminal halves of calmodulin make it very unlikely that they result from direct interaction with the peptide. More likely, the effects observed for the tryptophans in the calcium-binding loops result from long-range conformational changes upon peptide binding. It is important to note that these effects may be related to very subtle changes in the environment of the tryptophan residues. The physical basis of the quenching mechanism that leads for Trp-62 and Trp-99 to different states defined by a different lifetime is very speculative (see above). Better understanding of this mechanism and of the structural significance of the lifetime-defined states would provide insight in the nature of the peptide-induced conformational changes.

Another striking result is that, despite the differences in their sequences, both peptides induced similar changes in the fluorescence properties of the tryptophans located in the loops

(Table II). In an attempt to determine whether this effect was general, we analyzed the fluorescence changes for these tryptophans upon binding of a naturally occurring calmodulin-binding peptide, mastoparan (I-N-L-K-A-L-A-A-L-A-K-K-I-L-$NH_2$) (Malencik & Anderson, 1983). Unfortunately, the study was perturbed by the appearance of two peptide-binding sites in some of the tryptophan-containing calmodulins (T62W and S81W SYNCAMs). In the case of F99W SYNCAM, however, the observed stoichiometry was 1:1, and the changes in steady-state and time-resolved fluorescence were strikingly similar to those upon RS20F or RS20CK binding (not shown). Mastoparan has the ability to form an amphiphilic cationic helix (McDowel et al., 1985). Compactness of the calmodulin–peptide complex upon mastoparan binding has been observed (Yoshino et al., 1989; Matsushima et al., 1989), as in the case of MLCK-I (Heidorn et al., 1989) and PhK5 (Trewhella et al., 1990), which both can form an amphiphilic cationic helix. Presently, we cannot infer how the changes in the fluorescence features that we observed are related to the changes in the structure of calmodulin upon peptide binding. However, our data suggest that the effects observed might be general in the case of a peptide able to form an amphiphilic cationic helix and inducing compactness of calmodulin upon binding.

Close examination of the data reveals slight but significant differences in the fluorescence changes of the Trp located in the C-terminal calcium-binding loops upon the binding of RS20F and RS20CK. The emission maximum of Trp-135 is not altered upon RS20F binding, whereas it is 2-nm blue-shifted upon RS20CK binding (Table II). Fluorescence decay measurements also reveal a decrease in the longer lifetimes upon RS20CK binding compared to RS20F (Table V), which suggests some differences in the microenvironment of Trp-99, upon binding of RS20F or RS20CK. This suggests similar but somewhat different changes in the environment of these residues to optimize the interaction with peptides of different sequences.

On the molecular graphics, Trp-81 is widely accessible to solvent and near the hydrophobic region in the C-terminal half of the protein (not shown). The emission maximum of S81W SYNCAM, 344 nm, is markedly shifted as compared to Trp in water (356 nm) and is in apparent contradiction with the solvent exposure of Trp-81 on the graphics. This suggests a less polar, more restricted environment in solution than on the computer model. Whether this is related to the compactness of the folded solution structure suggested by the data of Heidorn and Trewhella (1988), we cannot infer at this point. A bend in the central helix could bring Trp-81 in the close vicinity of the C-terminal hydrophobic pocket, inducing a blue-shift of the spectrum compared to the Trp in water. Acrylamide quenching data, which show that the tryptophan is partially buried, support this model. It is noteworthy that the spectrum of this tryptophan is broader than that of Trp in water. This suggests heterogeneities in its environment, which might be related to the flexible structure of two lobes tethered at each end of a central helix (Persechini & Kretsinger, 1988; Persechini et al., 1989; Heidorn & Trewhella, 1988).

Peptides RS20F and RS20CK have markedly different effects on the fluorescence of S81W SYNCAM. Its emission maximum is 9-nm blue-shifted in the complex with RS20CK, as compared to that with RS20F (Table II), which suggests that the environment of Trp-81 in the former case is more hydrophobic than in the latter one. Quenching experiments show a decrease in the electrostatic repulsion between iodide and the environment of Trp-81 upon RS20F binding, strongly suggesting the existence of electrostatic interactions between calmodulin and RS20F in this region. This effect was not observed upon RS20CK binding. This is consistent with the observation that the activation of smooth muscle MLCK and that of calmodulin-dependent protein kinase II are differentially altered by the charge reversal of the negative cluster Glu 82–84 (Weber et al., 1989). While perturbation of Glu 82–84 has a major effect on the ability of calmodulin to regulate smMLCK, it does not affect the activation of CaMPK-II. The increased affinity of calmodulin for MLCK compared with that for CaMPK-II, which is evidenced by the higher calmodulin concentration required for activation in the latter case (Shoemaker et al., 1990), might be related, at least in part, to this difference in the binding mechanism.

It is noteworthy that four of the seven basic residues of RS20F, Arg-1, Arg-2, Lys-3, and Arg-16, are conserved in RS20CK (Table I). With the model of peptide binding proposed by O'Neil and DeGrado (1990), residues 4 and 14 of the peptides used in this study, which by sequence homology corresponds to residues 3 and 13 of the peptide studied by these authors, would interact with the C- and N-terminal hydrophobic cores. The homology between the peptides RS20F and RS20CK is limited to the N- and C-terminal part of their sequence (Table I). The central part of their sequence, from residue 4 to 15, is strikingly different, with three basic and five hydrophobic residues for RS20F and one basic and seven hydrophobic residues for RS20CK. These sequences suggest an increased role for electrostatic interactions in the complex of calmodulin with RS20F and increased role for hydrophobic interactions in that with RS20CK, which is consistent with our data. Work presently in progress should allow us to better characterize the residues of the peptides directly involved in binding to central helix. Our data provide evidence that the interaction of the two peptides with calmodulin is dramatically different in the region surrounding residue 81. This differential response of the central helix to the presence of CaM-binding peptides is consistent with the hypothesis that the central helix can play a differential role in the recognition of, or response to, CaM-binding structures.

## Acknowledgments

We thank Drs. T. A. Craig and D. M. Roberts for the construction, preparation, and characterization of the mutant calmodulins, Dr. P. E. Matrisian for the automated DNA sequence analysis, and Dr. J. Haiech for the preparation of the calmodulin mutants. We also thank Dr. M. C. Kilhoffer for communicating her results to us prior to publication and for stimulating discussion, Dr. Z. Bajzer for providing us with the fitting program for the acrylamide quenching experiments, Mr. B. J. Madden for the amino acid analysis of the calmodulin mutants and of the peptides, Mr. K. D. Peters for his help for the use of the computer facilities, and Ms. J. Kappers for expert editorial assistance.

**Registry No.** nmMLCK, 51845-53-5; Ca, 7440-70-2; protein kinase, 9026-43-1.

## References

Alcala, J. R., Gratton, E., & Prendergast, F. G. (1987a) *Biophys. J. 51*, 597–604.

Alcala, J. R., Gratton, E., & Prendergast, F. G. (1987b) *Biophys. J. 51*, 925–936.

Babu, Y. S., Sack, J. S., Greenhough, T. J., Bugg, C. E., Means, A. R., & Cook, W. J. (1985) *Nature 315*, 37–40.

Babu, Y. S., Bugg, C. E., & Cook, W. J. (1988) *J. Mol. Biol. 204*, 191–204.

Bakhshiev, N. G., Mazurenko, Y. T., & Piterskaya, I. V. (1966) *Opt. Spektrosk. 21*, 307–309.

Beechem, J. M., & Brand, L. (1985) *Annu. Rev. Biochem. 54*, 43–71.

Bevington, P. R. (1969) in *Data reduction and error analysis for the physical sciences*, McGraw-Hill, New York.

Blumenthal, D. K., Takio, K., Edelman, A. M., Charbonneau, H., Titani, K., Walsh, K. A., & Krebs, E. G. (1985) *Proc. Natl. Acad. Sci. U.S.A. 82*, 3187–3191.

Blumenthal, D. K., & Krebs, E. G. (1988) in *Calmodulin* (Cohen, P., & Klee, C. B., Eds.) pp 341–355, Elsevier, Amsterdam.

Brooks, B. R., Bruccoleri, R. E., Olafson, B. D., States, D. J., Savanirnathan, S., & Karplus, M. (1983) *J. Comput. Chem. 4*, 187–217.

Chabbert, M., Kilhoffer, M. C., Watterson, D. M., Haiech, J., & Lami, H. (1989) *Biochemistry 28*, 6093–6098.

Chang, M. C., Petrich, J. W., McDonald, D. B., & Fleming, G. R. (1983) *J. Am. Chem. Soc. 105*, 3819–3824.

Colbran, R. J., Fong, Y. L., Schworer, C. M., & Sodeerling, T. R. (1988) *J. Biol. Chem. 263*, 18145–18151.

Comte, M., Maulet, Y., & Cox, J. A. (1983) *Biochem. J. 209*, 269–272.

Cox, J. A., Comte, M., Malnoe, A., Burger, D., & Stein, E. A. (1984) *Met. Ions Biol. Syst. 17*, 215–293.

Cox, J. A., Comte, M., Fitton, J. E., & DeGrado, W. F. (1985) *J. Biol. Chem. 260*, 2527–2534.

Craig, T. A., Watterson, D. M., Prendergast, F. G., Haiech, J., & Roberts, D. M. (1987) *J. Biol. Chem. 262*, 3278–3284.

Eftink, M. R., & Ghiron, C. A. (1976) *Biochemistry 15*, 672–680.

Finazzi-Agro, A., Rotilio, G., Avigliano, L., Guerrieri, P., Boffi, V., & Mondovi, B. (1970) *Biochemistry 9*, 2009–2014.

Haiech, H., Klee, C. B., & Demaille, J. G. (1981) *Biochemistry 20*, 3890–3897.

Hanley, R. M., Means, A. R., Kemp, B. E., & Schenolikar, S. (1988) *Biochem. Biophys. Res. Commun. 152*, 122–128.

Hedstrom, J., Sedarous, S., & Prendergast, F. G. (1988) *Biochemistry 27*, 6203–6208.

Heidorn, D. B., & Trewhella, J. (1988) *Biochemistry 27*, 909–915.

Heidorn, D. B., Seeger, P. A., Rokop, S. E., Blumenthal, D. K., Means, A. R., Crespi, H., & Trewhella, J. (1989) *Biochemistry 28*, 6757–6764.

Herzberg, O., & James, M. N. (1985) *Nature 313*, 653–659.

James, P., Maeda, M., Fischer, R., Verma, A. K., Krebs, J., Penniston, J. T., & Carafoli, E. (1988) *J. Biol. Chem. 263*, 2905–2910.

Kilhoffer, M. C., Roberts, D. M., Adibi, A. O., Watterson, D. M., & Haiech, J. (1988) *J. Biol. Chem. 263*, 17023–17029.

Kilhoffer, M. C., Roberts, D. M., Adibi, A., Watterson, D. M., & Haiech, J. (1989) *Biochemistry 28*, 6086–6092.

Klevit, R. E., Blumenthal, D. K., Wemmer, D. E., & Krebs, E. G. (1985) *Biochemistry 24*, 8152–8156.

Kretzinger, R. H., Rudnick, S. E., & Weissman, L. J. (1988) *J. Inorg. Biochem. 28*, 289–302.

Lackowicz, J. R. (1983a) in *Principles of Fluorescence Spectroscopy*, pp 257–295, Plenum Press, New York.

Lackowicz, J. R. (1983b) in *Principles of Fluorescence Spectroscopy*, pp 383–428, Plenum Press, New York.

Lackowicz, J. R., & Cherek, H. (1980) *J. Biol. Chem. 255*, 831–834.

LaPorte, D. C., Wierman, B. M., & Storm, D. M. (1980) *Biochemistry 19*, 3814–3819.

Leto, T. L., Pleasic, S., Forget, B. G., Benz, E. J., & Marchesi, V. T. (1989) *J. Biol. Chem. 264*, 5826–5830.

Linse, S., Drakenberg, T., & Forsen, S. (1986) *FEBS Lett. 199*, 28–32.

Lukas, T. J., Burgess, W. H., Prendergast, F. G., Lau, W., & Watterson, D. M. (1986) *Biochemistry 25*, 1458–1464.

Malencik, D. A., & Anderson, S. R. (1983) *Biochem. Biophys. Res. Commun. 114*, 50–56.

Malencik, D. A., & Anderson, S. R. (1984) *Biochemistry 23*, 2420–2428.

Manalan, A. S., & Klee, C. B. (1984) in *Advances in Cyclic Nucleotide and Protein Phosphorylation Research* (Greengard, P., & Robison, G. A., Eds.) Vol. 18, pp 227–277, Raven Press, New York.

Mann, D. A., & Vanaman, T. C. (1988) *J. Biol. Chem. 263*, 11284–11290.

Matsushima, N., Izumi, Y., Matsuo, T., Yoshino, H., Ueki, T., & Miyake, Y. (1989) *J. Biochem. (Tokyo) 105*, 883–887.

Maulet, Y., & Cox, J. A. (1983) *Biochemistry 22*, 5680–5686.

McDowell, L., Sanyal, G., & Prendergast, F. G. (1985) *Biochemistry 24*, 2979–2984.

Newton, D. L., Oldewurtel, M. D., Krinks, M. H., Shiloach, J., & Klee, C. B. (1984) *J. Biol. Chem. 259*, 4419–4426.

Olwin, B. B., Edelman, A. M., Krebs, E. G., & Storm, D. R. (1984) *J. Biol. Chem. 259*, 10949–10955.

O'Neil, K. T., & DeGrado, W. F. (1990) *Proteins: Struct., Funct., Genet. 6*, 284–293.

O'Neil, K. T., Wolfe, H. R., Erickson-Viitanen, S., & DeGrado, W. F. (1987) *Science 236*, 1454–1456.

O'Neil, K. T., Erickson-Viitanen, S., & DeGrado, W. F. (1989) *J. Biol. Chem. 264*, 14571–14578.

Payne, M. E., Fong, Y. L., Ono, T., Colbran, R. J., Kemp, B. E., Soderling, T. R., & Means, A. R. (1988) *J. Biol. Chem. 263*, 7190–7195.

Persechini, A., & Kretzinger, R. H. (1988) *J. Biol. Chem. 263*, 12175–12178.

Persechini, A., Blumenthal, D. K., Jarret, H. W., Klee, C. B., Hardy, D. O., & Kretzinger, R. H. (1989) *J. Biol. Chem. 264*, 8052–8058.

Petrich, J. W., Chang, M. C., McDonald, D. B., & Fleming, G. R. (1983) *J. Am. Chem. Soc. 105*, 3824–3832.

Putkey, J. A., Draetta, G. F., Slaughter, G. R., Klee, C. B., Cohen, P., Stull, J. T., & Means, A. R. (1986) *J. Biol. Chem. 261*, 9896–9903.

Rasmussen, H., Kojima, I., Kojima, K., Zawalich, W., & Apfeldorf, W. (1984) in *Advances in Cyclic Nucleotide and Protein Phosphorylation Research* (Greengard, P., & Robison, G. A., Eds.) Vol. 18, pp 159–193, Raven Press, New York.

Ricci, R. W., & Nesta, J. M. (1976) *J. Phys. Chem. 80*, 974–980.

Roberts, D. M., Crea, R., Malecha, M., Alvarado Urbina, G., Chiarello, R. H., & Watterson, D. M. (1985) *Biochemistry 24*, 5090–5098.

Sanyal, G., Richard, L. M., Carraway, K. L., & Puett, D. (1988) *Biochemistry 27*, 6229–6236.

Seaton, B. A., Head, J. F., Engelman, D. M., & Richards, F. M. (1985) *Biochemistry 24*, 6740–6743.

Seeholzer, S. H., & Wand, A. J. (1989) *Biochemistry 28*, 4011–4020.

Shizuka, H., Serizawa, M., Shimo, T., Saito, I., & Matsuura, T. (1988) *J. Am. Chem. Soc. 110*, 1930–1934.

Shoemaker, M. O., Lau, W., Shattuck, R. L., Kwiatkowski, A. P., Matrisian, P. E., Guerra-Santas, L., Wilson, E., Lukas, T. J., Van Eldik, L., & Watterson, D. M. (1990) *J. Cell Biol. 111*, 1107-1125.
Stoclet, J. C., Gerard, D., Kilhoffer, M. C., Lugnier, C., Miller, R., & Schaeffer, P. (1987) *Prog. Neurobiol. 29*, 321-364.
Tanaka, T., & Hidaka, H. (1980) *J. Biol. Chem. 255*, 11078-11080.
Teleman, O., & Ahlstrom, P. (1986) *J. Am. Chem. Soc. 108*, 4333-4341.
Trewhella, J., Blumenthal, D. K., Rokop, S. E., & Seeger, P. A. (1990) *Biochemistry 29*, 9316-9324.
Wahl, P., & Auchet, J. C. (1972) *Biochim. Biophys. Acta 285*, 99-117.
Weber, P. C., Lukas, T. J., Craig, T. A., Wilson, E., King, M. M., Kwiatkowski, A. P., & Watterson, D. M. (1989) *Proteins: Struct., Funct., Genet. 6*, 70-85.
Werner, T. C., & Forster, L. S. (1979) *Photochem. Photobiol. 29*, 905-914.
Yazawa, M., Ikura, M., Hikichi, K., Ying, L., & Yagi, K. (1987) *J. Biol. Chem. 262*, 10951-10954.
Zimmer, W. E., Schoss, J. A., Silslow, C. D., Youngblom, G., & Watterson, D. M. (1988) *J. Biol. Chem. 263*, 19370-19383.

# Characterization of the Binding of Plasminogen to Fibrin Surfaces: The Role of Carboxy-Terminal Lysines†

Valérie Fleury and Eduardo Anglés-Cano*
*Institut National de la Santé et de la Recherche Médicale, U. 143, Hôpital de Bicêtre, IPC, F-94275-Cedex, Bicêtre, France*
*Received March 19, 1991; Revised Manuscript Received May 20, 1991*

ABSTRACT: In the present study we have quantitatively characterized the interaction of purified human Glu- and Lys-plasminogen with intact and degraded fibrin by ligand-binding experiments using a radioisotopic dilution method and antibodies against human plasminogen. A fibrinogen monolayer was covalently linked to a solid support with polyglutaraldehyde and was treated with thrombin or with thrombin and then plasmin to respectively obtain intact and degraded fibrin surfaces. Under these conditions, a well-defined surface of fibrin is obtained (410 ± 4 fmol/cm$^2$) and, except for a 39-kDa fragment, most of the fibrin degradation products remain bound to the support. New binding sites for plasminogen were detected on the degraded surface of fibrin. These sites were identified as carboxy-terminal lysine residues both by inhibition of the binding by the lysine analogue 6-aminohexanoic acid and by carboxy-terminal end-group digestion with carboxypeptidase B. The binding curves exhibited a characteristic Langmuir adsorption isotherm saturation profile. The data were therefore analyzed accordingly, assuming a single-site binding model to simplify the analysis. Equilibrium dissociation constants ($K_d$) and the maximum number of binding sites ($B_{max}$) were derived from linearized expression of the Langmuir isotherm equation. The $K_d$ for the binding of Glu-plasminogen to intact fibrin was 0.99 ± 0.17 μM and for degraded fibrin was 0.66 ± 0.22 μM. The $K_d$ for the binding of Lys-plasminogen to intact fibrin was 0.41 ± 0.22 μM and for degraded fibrin was 0.51 ± 0.12 μM. The $K_i$ for the inhibition of the binding by 6-aminohexanoic acid was 130 ± 15 μM on intact fibrin and 109 ± 18 μM on degraded fibrin. The total number of binding sites markedly increased upon degradation of the fibrin surface by plasmin: ~0.1 pmol of plasminogen was bound to intact fibrin while ~1 pmol was detected on the degraded surface. The plasminogen/fibrin ratio increased from 0.3 to 2.7 upon plasmin degradation. These data provide quantitative evidence of the amplification of fibrinolysis by carboxy-terminal lysine residues unveiled by plasmin on the surface of fibrin and support the concept of fibrinolysis as a surface-controlled process.

Physiological fibrinolysis involves heterogeneously catalyzed reactions that proceed at the fibrin/plasma interface, where fibrin provides a surface to which tissue plasminogen activator (t-PA)[1] [EC 3.4.21.31] and plasminogen adsorb in a sequential and ordered manner (Wiman & Collen, 1978; Hoylaerts et al., 1982). Molecular assembly of these proteins results in a ternary complex that efficiently generates plasmin [EC 3.4.21.7] on the surface of fibrin and thereby triggers the dissolution of a clot. It has been recently suggested that early fibrin degradation accelerates fibrinolysis by increasing the binding of both t-PA and plasminogen to new binding sites created by plasmin on the surface of fibrin (Suenson et al., 1984; Tran-Thang et al., 1984; Harpel et al., 1985; Higgins & Vehar, 1987). This mechanism is mediated by specific interactions of lysine residues in fibrin with the kringle domains of plasminogen (Varadi & Patthy, 1983; Nieuwenhuizen et

† This work was supported by INSERM and by a research grant from NATO; V.F. is a recipient of a scholarship from the Ministère de la Recherche et de la Technologie.
* To whom correspondence should be addressed.

[1] Abbreviations: Glu-plasminogen, native human plasminogen with N-terminal glutamic acid; Lys-plasminogen, plasmin-modified forms of Glu-plasminogen with N-terminal lysine, valine, or methionine (mostly lysine) obtained by hydrolysis of the Arg-68-Met-69, Lys-77-Lys-78, or Lys-78-Val-79 peptide bonds; t-PA, tissue-type plasminogen activator; CBS 1065, chromogenic substrate (methylmalonyl)hydroxyprolyl-arginine-*p*-nitroanilide; S-2366, chromogenic substrate L-pyroglutamyl-L-prolyl-L-arginine-*p*-nitroanilide; 6-AHA, 6-aminohexanoic acid; AMCHA, *trans*-4-(aminomethyl)cyclohexanecarboxylic acid; VPL, dansyl-valyl-L-phenylalanyl-L-lysine chloromethyl ketone; PPACK, dansyl-phenylalanyl-L-prolyl-L-arginine chloromethyl ketone; EDTA, ethylenediaminetetraacetic acid; DFP, diisopropyl fluorophosphate; SDS, sodium dodecyl sulfate.

0006-2960/91/0430-7630$02.50/0 